Modelling medulloblastoma pathogenesis and treatment in human cerebellar organoids.

Thomas Willott[1], James G Nicholson[1], Yunchen Xiao[1], Olumide Ogunbiyi[2], Talisa Mistry[2], Nicolae Radu Zabet[1], Ashirwad Merve[2], Sara Badodi[1]* & Silvia Marino[1,3]*

[1] Brain Tumour Research Centre, Blizard Institute, Queen Mary University of London, London (UK)

[2] Department of Histopathology, Great Ormond Street Hospital for Children NHS Foundation Trust, Great Ormond Street, London (UK)

[3] Barts Brain Tumour Centre, Queen Mary University of London and Barts Health, London (UK)

*shared senior and corresponding authors: s.badodi@qmul.ac.uk and s.marino@qmul.ac.uk

Graphical Abstract

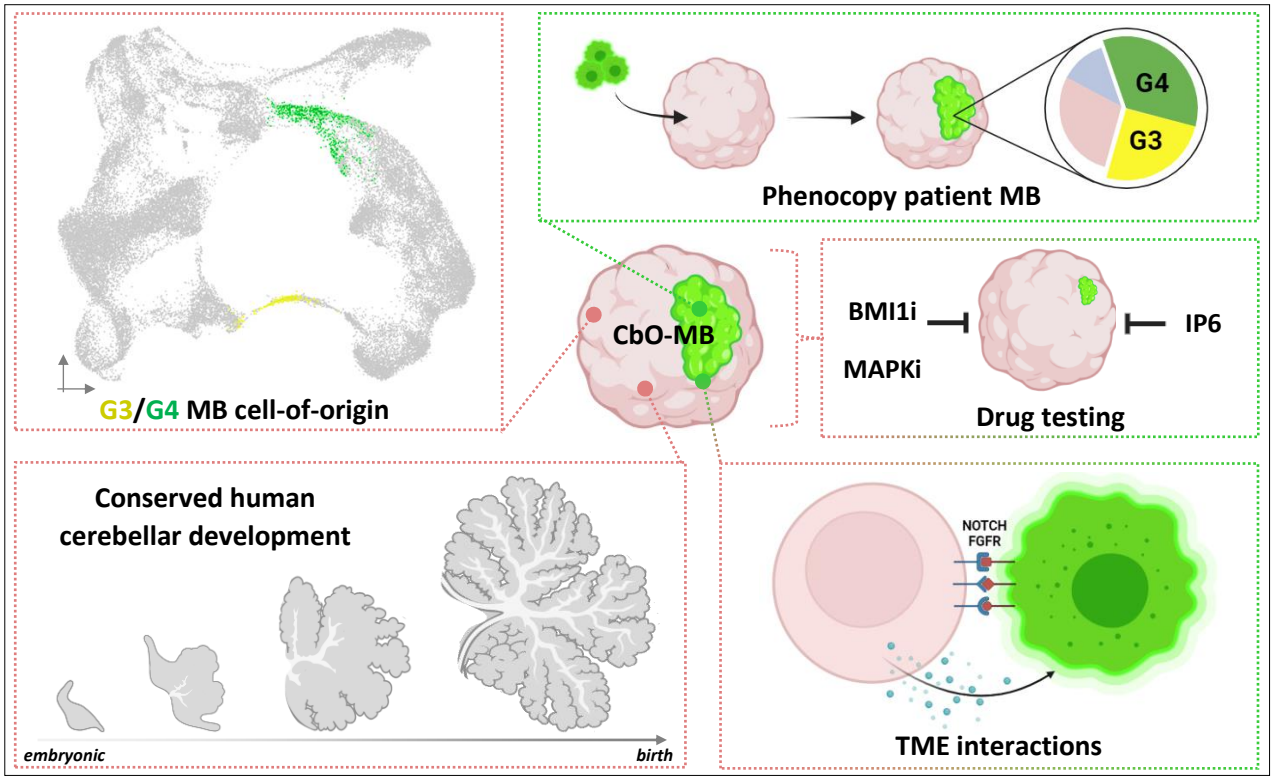

Image created with BioRender.

Abstract

Faithful genetically engineered *in vivo* models of medulloblastoma (MB) are currently available only for some molecular subgroups, in keeping with recent studies showing the unique role of human-specific progenitors in the development of G3 and G4 MB subgroups. We generated human cerebellar organoids (CbO) from expanded potential stem cells (EPSC) and characterised in depth their epigenetic and transcriptomic profile. We show the presence of sub compartment-specific cerebellar lineages linked to MB formation, including populations expressing signature genes of G3 and G4 MB cells-of-origin in a 1 month-old CbO. Moreover, we demonstrate that CbO sustains MB cells proliferation and invasion in a 3D co-culture model (CbO-MB) while preserving their molecular identity, and that treatment of CbO-MB with anti-tumour compounds recapitulate the efficacy of *in vivo* drug testing in PDX models.

Introduction

Medulloblastoma (MB) is a cerebellar tumour accounting for the largest proportion of brain cancer diagnoses in children. Molecular subgrouping based on transcriptomic, epigenomic and genomic features have collectively identified 4 MB subgroups: SHH (Sonic Hedgehog), WNT (Wingless-related Integration Site), Group 3 (G3) and Group 4 (G4), each further divided into subtypes with distinct prognosis and responses to therapy [1-4]. Despite these advances in classification, MB standard of care remains unchanged, with patients undergoing surgical resection followed by chemotherapy and/or radiotherapy [5], which albeit effective in a majority of patients, is associated with significant and in many cases life changing side effects.

SHH and WNT MB are well understood due to their clearly characterised origin and defined molecular alterations, leading to a surge in the development of molecularly targeted and/or immunotherapies in *in vitro* and *in vitro* models, translating into early-phase clinical trials for patients in these subgroups in recent years [6]. The unclear origin and lack of universal pathway aberrations in G3/G4 MB subgroups with consequent lack of faithful pre-clinical models has hampered the identification of new treatment options for these patients [7]. In particular, *in vitro* models for G4 MB, the most common MB subgroup, are highly underrepresented compared to other subgroups due to difficulties establishing 2D cell culture, whilst currently available G3 MB cell lines predominantly harbour *MYC* amplifications without encompassing the heterogeneity seen in these tumours [8,9]. The successful direct transplantation and maintenance of primary MB tumour cells as patient derived orthotopic xenograft (PDX) models has overcome some of these issues [10-12], however the cost and resources required for these models limit their broader applications and scalability for drug testing.

Taking into account that MB are neoplasms closely linked to deregulated cerebellar development [13], the recent identification of the putative cells of origin of G3/G4 subgroups [14,15] may represent a significant step forward. Spatiotemporally restricted mitotic glutamatergic neuron progenitors harbouring photoreceptor (PRC) and unipolar brush cell (UBC) gene signatures were identified as G3 and G4 MB cells of origin respectively by mapping lineage trajectories from MB single cell RNA sequencing (scRNA-Seq) data to human foetal cerebellar development. These progenitors are halted in development prior to cell cycle exit leading to malignancy [14].

Importantly, immunohistochemical and pseudo-time comparisons of relevant stages of cerebellar development between human and mice showed significantly fewer of these proliferative progenitors in mice, raising the possibility that genetically engineered mouse models may not allow the study of key features of G3/G4 MB, including for example their onset [15].

Advances in organoid research have enabled the generation of new tools to study various aspects of cancer biology, including tumour initiation [16], metastasis [17] and as a co-culture model for drug testing [18], with important implications for personalised medicine [19]. Methods to generate cerebellar organoids (CbO) from induced pluripotent stem cells (iPSCs) have been developed [20,21] and characterised at single cell transcriptome level, achieving neuronal and glial differentiation with cerebellar sub-compartment identity [22-24]. In the context of MB modelling, current applications of CbO are restricted to studies of neoplastic transformation in genetically engineered organoids which lacked any specificity for their respective cell-of-origin hence requiring subsequent injection in mouse models to achieve the formation of a tumour [25,26].

Here, we have generated for the first time a human CbO from expanded potential stem cells (EPSCs) and assessed their suitability to model G3/G4 MB by investigating whether they contain their cell-of-origin at stages of differentiation comparable to foetal cerebellar development as assessed by dating at single cell transcriptome and DNA methylation level. In addition, we have analysed its suitability as a co-culture model of G3/G4 MB cells and as a pre-clinical drug testing tool.

Methods

Cell Culture

EPSC61 and EPSC19 were cultured as described previously [19] on plates coated in Geltrex (Life Sciences) in mTEsR plus basal media (StemCell Technologies). During routine passaging, cells were detached with 0.1 mM EDTA (Life Sciences) and re-plated with media supplemented with 10 μM Y-27632 Dihydrochloride (PeproTech, #1293823). CHLA-01-Med primary and CHLA-01R-Med recurrent MB cell lines purchased from ATCC were cultured in suspension in Gibco DMEM-F12 media (Life Technologies) supplemented with 20 ng/mL human recombinant FGF and 20 ng/mL human recombinant EGF (Peprotech), 2% B-27 supplement (Invitrogen) and 1% Penicillin-Streptomycin. ICb1299 primary MB cells obtained from Dr Xiao-Nan Li, Baylor College of Medicine, Texas Children Cancer Centre, USA [11,27] were cultured semi-adherently in Gibco DMEM media (Life Technologies) supplemented with 10% foetal bovine serum (Gibco) and 1% Penicillin-Streptomycin (Life Sciences).

All cell lines were confirmed mycoplasma negative prior to experimental procedures and cultured in humidified incubators at 37°C with 5% CO2 until ~80% confluent before passaging.

Cerebellar Organoid Culture

Cerebellar organoids were cultured based on a previously published protocol [16]. Briefly, EPSCs at 80% confluency were detached using gentle cell dissociation reagent (StemCell) and plated into 96-well ultra-low attachment V-bottomed plates (PHCBI) in mTEsR plus basal media (StemCell) supplemented with 10uM Y-27632 Dihydrochloride (PeproTech, #1293823) at 6,000 cells per well. On Day 1, media was replaced with mTEsR plus basal media. On Day 2, media was replaced with growth-factor free chemically defined media (gfCDM) containing: IMDM (Life Technologies)/Ham's F-12 (Life Technologies) 1:1, 1% v/v chemically defined lipid concentrate (Life Technologies), 450 μM monothioglycerol (Sigma), 15 μg/ml apo-transferrin (Sigma), 5 mg/ml crystallization-purified BSA (Sigma), 50 U/ml penicillin/50 μg/ml streptomycin and 7 μg/ml insulin (Sigma). On Day 2-7, 50 ng/ml human recombinant FGF2 (PeproTech, #100-18B) and 10 μM SB431542 inhibitor (Life Sciences, #S4317) were added to gfCDM. On Day 7, organoids were transferred to 6-well ultra-low attachment plates (Corning) on an orbital shaker (120 rpm) in a humidified incubator at 37°C with 5% CO2 where they were maintained for the

remainder of the protocol. For Day 7-14, 33.3 ng/ml human recombinant FGF2 and 6.67 μM SB431542 inhibitor were added to gfCDM, then 100 ng/ml human recombinant FGF19 (PeproTech, #100-32) was added to gfCDM for Day 14-21 of culture. From Day 21, organoids were cultured in complete neurobasal media containing: Neurobasal medium (Life Technologies), GlutaMax I (Life Technologies), N2 supplement (Life Technologies), and 50 U/ml penicillin/50 μg/ml streptomycin. 300 ng/ml human recombinant SDF1 (PeproTech, #300-28A) was added to complete neurobasal media from Day 28-35.

CbO-MB co-culture

On Day 35 of CbO culture, organoids were placed in 96-well ultra-low attachment U-bottomed plates (Corning) in a 1:1 mix of complete MB cell media and complete neurobasal media with 100,000 MB cells infected with shCHD7 lentivirus containing GFP as previously published [28]. The following day, half media from each well was replaced with complete neurobasal media. On Day 37, the entire contents of each well was transferred to a 24-well ultra-low attachment plate (Corning) with 1ml complete neurobasal media. On Day 4, total media was replaced with complete neurobasal media to remove non-infiltrating cells and organoids placed back on the orbital shaker (120 rpm) in a humidified incubator at 37°C with 5% CO2. Co-cultures were maintained for 14 days in total from MB cell seeding before taking for drug assays or scRNA-Seq.

Human Cerebellar FFPE Samples Processing

12 human cases from Great Ormond Street Hospital (GOSH) at pre-natal developmental timepoints were selected as having normal cerebellar histology and consent for research. Areas of tissue containing cerebellar material were identified and manually macro dissected according to the marking shown in Figure S2A. Following dissection, tissue was kept at -20°C until downstream processing.

DNA/RNA Extraction

For CbO samples, DNA and RNA were extracted using the RNA/DNA/Protein Purification Plus kit (Norgen) following manufacturer protocol. For FFPE human cerebellar samples, initial deparaffinization and DNA extraction was performed using FFPE RNA/DNA Purification Plus Kit (Norgen). Samples were incubated with Proteinase K overnight at 37°C to increase yield, after which DNA extraction was performed as per manufacturer instructions.

RT-qPCR

All cDNA synthesis was performed using the SuperScript III Reverse Transcriptase kit (Invitrogen) according to the manufacturer's protocol. Analysis of gene expression was carried out using the Applied Biosystems 7500 Real-Time PCR with SYBR Green PCR MasterMix (Applied Biosystems) according to standard protocols. All qPCR were performed in triplicate with 10ng cDNA. Average Ct values for target genes were normalised to average Ct of ACTIN B and GAPDH housekeeping genes before calculating fold change. Primers used are listed in Table 1.

Immunohistochemistry (IHC)

Organoids were collected and fixed in 4% PFA in PBS, dehydrated in 30% sucrose in PBS and embedded in blocks of 7.5% gelatin, 10% sucrose in PBS. Blocks were then snap frozen in isopentane at -55°C before cryosectioning at 15 µm sections. Prior to staining, sections were de-gelatinised in warm water before permeabilisation in 4% normal donkey serum with 0.25% Triton-X in PBS for 2 hours. Sections were then washed in PBS before incubation with primary antibodies at 4°C overnight diluted in 4% normal donkey serum in PBS. A list of primary antibodies and dilutions are shown in Table 2. Sections were then washed 3 times in PBS followed by incubation for 3 hours at room temperature with corresponding AlexaFluor™ secondary antibodies at 1:500 dilution in PBS. After a final 3 PBS washes, sections were mounted with coverslips using ProLong™ Gold antifade reagent with DAPI (Thermo Fisher Scientific, P36931). Images were taken using Zeiss 800 Laser Scanning Confocal microscope with Zeiss ZEN software v2.3.

CbO-MB drug assays

On Day 0 of drug assays, CbO-MB were transferred to new 24-well ultra-low attachment plates (Corning) containing 500 µL complete neurobasal media plus drug PTC-209 and PD325901 inhibitors or DMSO vehicle then placed back on rotary shaker where they remained for the duration of the assay. A drug and media top up was performed on day 2.

On day 4, the entire contents of each well was collected and the Neural Dissociation kit (MACS Miltenyi Biotec) was used to dissociate treated CbO-MB co-cultures into single cell suspension. Samples were then stained with the Zombie NIR™ Fixable Viability Kit (Biolegend) at 1:300 dilution, after which all samples were analysed using the BD LSRII flow cytometer. GFP expressing cells were detected with the blue excitation laser at 488nm, while the Zombie NIR positive cells were detected with the red excitation at 633nm. Upon gating of single cells, Zombie NIR positive cells were

gated as dead, with GFP fluorescence distinguishing viable MB from CbO cells. Full details of FACS gating strategy with example plots can be found in Supplementary Methods. All subsequent FACS analysis was performed in FlowJo v10.6.2.

Dissociation of CbO and CbO-MB for scRNA-Seq

Pooled samples of CbO were taken at day 7 and day 35, as well as CbO-MB at day 49. First, organoids were dissociated using the Neural dissociation kit (MACS Miltenyi Biotec) into single cell suspension. Subsequent debris removal was then performed using Debris removal solution according to manufacturer protocol (Miltenyi Biotec, #130-109-398) to obtain a clean sample of highly viable cells. Cells were resuspended in loading buffer (0.04% BSA in PBS), strained through a 70 µm cell strainer and counted using a hemacytometer with trypan blue staining.

scRNA-Seq Analysis

Library preparation was performed at the Single Cell Genomics Facility (UCL, Cancer Institute) using the Chromium Next GEM Single Cell 3' Kit v3.1 (10X Genomics, 1000268) along with the Chromium Next GEM Chip G Single Cell Kit (10X Genomics, 1000120) according to the manufacturer's instructions. Pooled samples libraries were sequenced with lane sequencing on Novaseq 6000 S4 (Novogene). The Cell Ranger 2.0.1 pipeline was used to align reads to the GRCh38 human reference genome and produce count matrices for downstream pre-processing and analysis using the Seurat v5.0.1 R package [29].

UMAP calculations and cell type annotations

For stringent quality filtration, only cells with fewer than $5x10^4$ total reads, lower than 10% mitochondrial reads and more than 750 detected features were retained for analysis. Expression values were library size corrected to 10,000 reads per cell and log1p transformed, with Principal component analysis (PCA) performed on the scaled data for the top 2000 variable genes. For analysis of Day7 samples, batch correction between cell lines was performed on principal components using Harmony [30]. Uniform Manifold Approximation Projection (UMAP) embeddings, Nearest Neighbours and cell clusters were then calculated in harmony-corrected PCA space using 35 dimensions, and cells were clustered using FindClusters() with a resolution of 0.2. For Day 35-49, where the UMAP indicated a greater degree of cell type complexity, we used a FindClusters() resolution of 0.5. Cluster marker genes were calculated using a Seurat's in-bult Wilcoxon Rank Sum test (logfc.threshold = 0.25, min.pct = 0.1, only.pos = T), and differential expression analysis across experimental conditions was

performed using MAST [31]. Initial clustering identified two clusters 13 and 14 which represented hypoxic/glycolytic cells, common to all human brain organoids [32]. As has been done previously [33], these cells were excluded from analyses and a new UMAP was calculated. For analysis of co-cultures containing medulloblastoma (MB) cells, we changed the detected feature threshold to 500, and no batch correction was necessary. UMAPs and Nearest neighbours were calculated using 15 PCA dimensions and FindClusters() was run with a resolution of 0.35. We used InferCNV to distinguish between organoid and MB cells on the basis of genotype using the "subclusters" analysis mode, and setting the following parameters: cutoff=0.1, k_obs_groups = 2, leiden_resolution = $1x10^{-6}$. For annotating organoid cells from co-cultures we used the processed R object from the day 35-49 cerebellar organoids (Fig1B) as a reference, and the default settings of Seurat FindTransferAnchors(), TransferData() and AddMetaData() functions. We then annotated new cluster names based on their composition of transferred cell type labels Fig S2D-G. For the analysis of MB cells alone, cells identified by InferCNV were subset, and reanalysed using the standard Seurat pipeline; UMAPs and nearest neighbours were calculated using 10 PCA dimensions and FindClusters() was run with resolution=0.2.

scRNA-Seq Analysis: Comparison to reference datasets

To approximate the transcriptomic age of our CbOs we compared data from this study, and three other cerebellar organoid studies: Nayler et al [23], Chen et al [24], and Atamian et al [22] against three datasets derived from developing foetal cerebellum: Aldinger et al [34], Luo et al [35], and Zhong et al [36]. First, pseudo-bulk transcriptomic data were generated from aggregated single cells counts for all samples, and expressed as log(counts per million +1). Data was merged and batch correction between studies was performed using Combat() from the sva.3.48 package. We next derived an 'ageing-signature' as the top 200 genes correlated with age across the foetal cerebellum samples and used the signature to perform Pearson correlation between Cerebellar organoid and foetal cerebellum samples. To aid with cell type annotations, we compared cluster marker signatures against those from the three foetal cerebellum datasets. In each case we obtained published count matrices, UMAP-embeddings and author-defined cluster meta data, and used them to perform a Wilcoxon Rank Sum test (logfc.threshold = 0.25, min.pct = 0.1, only.pos = T) to obtain the list of cluster marker genes for their cell types. Then, for each dataset and marker gene, cluster specificity scores were computed (mean normalized counts per cluster/total mean

normalized counts) – with gene signature specificity scores compared across studies by Pearson correlation.

To compare MB cells in co-cultures to patient tumours, we generated pseudo-bulk transcriptomic data from aggregated single cells counts from our co-cultured MB samples, and 36 patients in Hovestadt et al [37]. Combat batch correction was performed between log(cpm+1) data, and Pearson correlation between samples were calculated across the top 1500 most variable genes (ranked by standard deviation). Pearson correlation across the same gene list was also used to query the relative similarity between patient tumours and MB cells, here sequenced after co-culture, and when we previously cultured them *in vitro* [28].

For reference signature scoring, average gene module expression was calculated for each single cell, subtracted by the aggregated expression of a random control set of features selected from the same average expression bins as the query genes [38]. G/S and G2M gene modules are included in the Seurat v5.0.1 package; G3 RL.PRC and G4 RL.UBC Medulloblastoma cell of origin signature were taken from Smith et al [14]; WNT SHH and G3/4 signatures were taken from Hovestad et al, as were three signatures (A, B & C) for cell states of G3/4 medulloblastomas [37].

Cell lineage trajectory analysis

For RNAvelocity analysis, velocyto [39] was used to calculate spliced and unspliced transcriptomes, before subsequent analysis using scVelo [40], on Seurat-defined cell types and UMAP embeddings, using default parameters. For single cell lineage trajectory analysis, we imported the processed Seurat object into the Monocle3 R package, and subset to cell types involved in the G3 trajectory (RL/NSCs, eCN progenitors and eCN) or G4 trajectory (NSCs, Glut. neuron progenitors and Granule/UBC) [41]. For each subset, the 'learn_graph' function was applied to infer single cell trajectories setting minimal_branch_len to 18 and the 'order_cells' function was used to selectRL/NSCs and NSCs as the root states of Pseudotime. Differential gene expression was calculated across single cell trajectories using Moran's I test. For each trajectory, the top 2500 most differentially expressed genes over pseudotime were selected, and smoothened, alra-imputed [42] expression over pseudotime was plotted.

Receptor Ligand Modelling

For receptor-ligand analysis, cell type meta data and count data for the top 5000 most highly variable gene was input into CellphoneDB v2.0 [43] and run using the

statistical_analysis mode. For circos plot visualization the Circlize v0.4.15 R package was used and only those significant receptor-ligand interactions that involved MB cells were included in the plot.

DNA methylation analysis

All CbO and human cerebellar DNA samples underwent standard BSC conversion at UCL Genomics facility (UCL, Great Ormond Street Institute of Child Health) and were submitted for Illumina Methylation EPIC v2 array following standard protocols. Quality control was performed and probe beta values were extracted from raw .idat files using wateRmelon R package [44] under reference genome hg38. Probes with detection p-values greater than 0.05 were removed using pfilter(), as well as probes associated with sex chromosomes, mitochondrial chromosomes and single nucleotide polymorphisms. Adjusted Dasen normalisation was then performed.

Cerebellar Organoid developmental staging (DNA methylation)

To stage the development of CbO compared with human cerebellar samples, a similar 'ageing signature' approach was applied, with the top 1% of probes whose beta values best correlated to age in human cerebellar samples selected for subsequent correlation with CbO probe betas. To corroborate this approach, CbO methylation data adapted to EPIC v1 array probe annotation was also passed to the foetal brain clock (FBC), an R package specifically trained on foetal brain samples during development to estimate their epigenetic age [45].

Differentially and variably methylated probes and regions Analysis

Differentially methylated probes (DMPs) and regions (DMRs) were calculated pairwise for CbO samples between Day 7 and later timepoints using the R package DMRcate [46] with FDR threshold of 0.01. Additional criteria for DMR identification were set such that DMRs must contain at least 6 CpG sites with <400 base pair separation. For human rhombic lip (RL) and external granular layer (EGL) correlation, raw .idat files for micro-dissected RL and EGL samples were accessed from GSE207266 [14] and processed using the same raw data processing pipeline adapted for EPIC v1 array annotation before downstream analysis. DMPs were identified between each cerebellar compartment (n=7) as stated above with FDR threshold of 0.01. DMPs were then subset to CbO average probe betas adapted to EPIC v1 array annotation and correlated to each cerebellar compartment.

Variable methylated probes (VMPs) and regions (VMRs) across all 5 CbO timepoints were identified within the DMRcate package using the same thresholds as stated

above for DMR analysis and the top 5% VMP/VMRs defined as significant. For human VMR analysis, average betas for RL/EGL samples were calculated for each developmental timepoint then integrated with the 12 human cerebellar samples from GOSH. Common probes adapted to EPIC v1 array were then identified and batch correction performed using ComBat for each study, then VMRs across human foetal cerebellar development calculated. VMRs were then annotated to genes (VMGs), after which significant VMGs were clustered based on z-scores of average beta-values of the probes contained within them and taken for pathway analysis.

scRNA-Seq/DNA methylation integration and pathway analysis

Differentially expressed genes (DEGs) between Day 7 and Day 35 CbO scRNA-Seq data with adjusted p-value < 0.05 and absolute log2FC > 0.25 were integrated with genes mapping to DMRs from methylation data at matched timepoints with p-value < 0.05 and greater than a 10% imposed threshold in methylation difference. Genes demonstrating concordant hypermethylation and down-regulation or hypomethylation and up-regulation were taken for subsequent pathway analysis. For pathway analysis, gene lists were input into Gprofiler [47] and pathways calculated based on a Benjamini-Hochberg FDR < 0.05. Pathway visualisation was performed using CytoScape [48]. For scRNA-Seq upon MB co-culture pathway analysis, UMAP clusters were grouped based on cell developmental state (un/differentiated) and effect of MB co-culture on cluster percentage (increase/decrease). Common pathways from each group were then identified and the top 100 most significant (adjusted-p<0.05) Reactome and KEGG pathways were plotted. For VMR pathway analysis, the top 100 most significant (adjusted-p<0.05) GO:Biological Process and GO:Molecular Function pathways were plotted for human and CbO VMG clusters, whilst for overlapping pathways with concordant DMR/DEG integration of Day 7 vs Day 35 CbO samples, GO:Cell Compartments were also plotted.

Ethics

Ethical approval for the work on human cerebellar samples obtained from GOSH was obtained from Brain UK, reference number 22/010.

Table 1 Primers used for RT-qPCR reactions

Gene	Forward Primer (5'-3')	Reverse Primer (5'-3')
ACTIN B	GCGAGAAGATGACCCAGATC	CCAGTGGTACGGCCAGAGG
GAPDH	CAATGACCCCTTCATTGACC	GACAAGCTTCCCGTTCTCAG
NESTIN	GAAACAGCCATAGAGGGCAAA	TGGTTTTCCAGAGTCTTCAGTGA
SOX1	TGCTTGTTCTGTTAACTCAC	AAAGAACCTCAGAGAGAGTC
EN2	CCGGCGTGGGTCTACTGTA	GGCCGCTTGTCCTCTTTGTT
OTX2	AGAGGACGACGTTCACTCG	TCGGGCAAGTTGATTTTCAGT
KIRREL2	ACAACTCTCCTTATGGTCATC	ATTCGCATCAGGTTCTTTTG
OLIG2	GACAAGCTAGGAGGCAGTGG	CGGCTCTGTCATTTGCTTCTTG
CORL2	CCAGGTGTTAAAAGGAAACACA	GCTCCCTTTTCATCTGATCCT
PAX6	AGAGAATACCAACTCCATCAG	GATAATGGGTTCTCTCAAACTC
ATOH1	TGTTATCCCGTCGTTCAACAAC	TGGGCGTTTGTAGCAGCTC
BARHL1	GAGCGGCAGAAGTACCTGAG	GTAGAAATAAGGCGACGGGAAC
EOMES	CACATTGTAGTGGGCAGTGG	CGCCACCAAACTGAGATGAT
GPR126	GATGGATTTTGAGAGTGGAC	GGAAAAGTCCAGTTTTGTTG

Table 2 Primary antibodies and dilutions used for immunohistochemistry

Primary Antibody	Dilution
SOX2 (abcam, ab97595)	1:500
OLIG2 (Santa Cruz, sc-19967)	1:200
CALB (Swant, CB300)	1:200
NeuN (Chemicon, MAB377)	1:500
EOMES (Chemicon, AB15894)	1:200
Ki67 (abcam, ab15580)	1:500
GFP (Chemicon, AB16901)	1:400

Results

CbO display a cellular composition recapitulating human cerebellar development.

We generated human CbO from two independent expanded potential stem cell (EPSC) lines (CbO_1 and CbO_2) obtained from reprogramming of dura mater fibroblasts [19] by modifying published protocols previously used only with iPSC (Figure 1A and S1Aa). 6000 cells were induced to differentiate and maturation was followed for 35 days as reported previously (Figure S1A), observing a significant increase in organoid size (Figure S1A,B) and the formation of characteristic flat-oval neural rosettes (Figure 1B) [20,21]. Expression of the stemness marker *NANOG* showed a significant decrease upon day 7 (D7) indicating that EPSCs in the aggregate lost their pluripotency and committed to differentiate (Figure S1C). Analysis of key genes for early cerebellar morphogenesis (Figure 1A) showed sustained expression from D7-14 of the neural stem cell markers *NESTIN* and *SOX1*, the cerebellar homeobox gene *EN2* [49] and *OTX2* transcription factor which is required during cerebellar development for signalling with the isthmic organiser [50] (Figure 1C and Figure S1D). To investigate differentiation into cerebellar GABAergic and glutamatergic neuronal populations, markers of mitotic progenitors and post-mitotic precursor populations were analysed during organoid maturation. We observed increased expression of *KIRREL2*, expressed in GABAergic progenitors, *OLIG2*, a marker of more mature GABAergic progenitors, and *CORL2, a* marker of post-mitotic Purkinje cell (Figure 1C and Figure S1E). Similarly, the glutamatergic progenitor marker *PAX6* and granule progenitor and precursor markers *ATOH1* and *BARHL1* showed increased expression during CbO maturation. Interestingly, the transcription factor *EOMES*, expressed specifically in glutamatergic progenitors with its expression sustained in unipolar brush cells (UBC) [51], was expressed both in early (D7) and late (D28-35) phases of the organoid maturation (Figure 1C and Figure S1F). Presence of GABAergic and glutamatergic granule neurons was also confirmed by expression of CALBINDIN and Neu-N proteins respectively, proximal to SOX2-positive neural rosette in mature CbO (Figure 1D and 1E). Finally, we detected expression of *GPR126*, a gene expressed during Bergmann glia development (Figure 1C and Figure S1G). These data show that CbO obtained from EPSC display the main cell types found in human cerebellum.

To characterise more in depth the cellular composition of CbO we performed single-cell RNA sequencing (scRNA-Seq) on 10,000 cells from a pool of 5 organoids obtained from two independent EPSC lines (CbO_1 and CbO_2) at D7, D35 and D49 timepoints to capture both the earliest and more mature stages of cerebellar progenitor development and neurogenesis (Figure 1F). To investigate cellular complexity during early CbO development (D7) we performed dimension reduction and Louvain clustering, visualizing cells as a Uniform Manifold Approximation and projection (UMAP). Although CbO cell diversity at this stage was limited, we could already identify three broad clusters in cycling/mitotic phase (Figure S1H) corresponding to *PAX6*$^+$/*OTX2*$^+$ glutamatergic progenitors, *PAX2*$^+$/*PAX5*$^+$/*PKDCC*$^+$ GABAergic progenitors and SOX9$^+$/S100B$^+$ glial progenitors, and even a small population of early *NEUROD4*$^+$/*NEUROG1*$^+$ neurons suggesting an initial lineage commitment (Figure S1I and S1J). By D35-49 there was a greater degree of cellular diversity and we identified 14 clusters (Figure 1G) that were annotated based on their expression of marker genes (Figure 1H) and correlations to endogenous cell types from reference datasets of the human developing cerebellum (Figure S1K) [34-36]. We found *VIM*$^+$, *HES1*$^+$, *SOX2*$^+$ and *NES*$^+$ stemness clusters including *MKI67*$^+$, *CCNB1*$^+$, *PCNA*$^+$ cycling stem, *OTX2*$^+$ hindbrain- and *IGFBP5*$^+$, *PAX3*$^+$, *PAX6*$^+$ RL-derived NSC; together with *GRID2*$^+$, *HES1*$^+$ and *IRX3*$^+$ NSC. We then observed a neuronal cluster for the GABAergic lineage of *SKOR2*$^+$, *LHX1*$^+$, *TFAP2*$^+$ and *CA8*$^+$ Purkinje cells. We also found several clusters associated with glutamatergic lineage including *OLIG3*$^+$, *ATOH1*$^+$ and *BARHL1*$^+$ glutamatergic progenitors and granule/UBC cluster expressing *MEIS1*, *IRX3* and *NEUROD1*. Interestingly, we noted increased expression of the UBC marker *EOMES* in these heterogeneous clusters, whilst specific granule progenitor cells (GPC) expressing *LHX2* and *NEUROD6* along with more mature granule cells expressing *SCG2* were also identified. Moreover, we identified clusters related to excitatory cerebellar nuclei (eCN) progenitors expressing *PAX6*, *NRN1* and *NHLH1*, as well as more mature eCN expressing *KCNIP4*, *MEIS3* and *NRN1*. In addition to lineages derived from glutamatergic and GABAergic neurons, we also identified other hindbrain clusters containing cell types contributing to cerebellar development, including *FOLR1*$^+$, *CFAP126*$^+$ and *RSPH1*$^+$ ependymal/choroid plexus, *POST*$^+$, *PRRX1*$^+$ and *COL1A1*$^+$ meninges and *SLIT2*$^+$, *GDF7*$^+$ roof plate (Figure 1H). Although we were not able to identify a homogeneous cluster representing glial differentiation,

we found increased expression of glial markers including *SLC1A3* and *FABP7* in a subset of cells within noncommitted NSC clusters (Figure 1H).

Our data show that the cellular composition of CbO recapitulates the main cell types found during cerebellar development.

Maturation of CbO follows conserved epigenetically regulated central nervous system developmental pathways.

Epigenetic regulation of gene expression plays a fundamental role during central nervous system (CNS) development [52] as it controls the spatio-temporal activity of cell lineage-specific genes. In particular, DNA methylation has been shown to robustly identify signatures, which enable lineage tracing of cells in development, tissue homeostasis and disease [53,54]. Hence, we analysed DNA methylation profiles of CbO and compared them with those of human foetal cerebellar samples between 19 and 37 post-conception weeks (PCW) (Figure S2A) to date the stage of development achieved in the CbO. We observed the highest correlation of the D35 CbO with 19 PCW cerebellum by comparing methylation profiles of the top 1% of CpG probes with positive linear correlation of methylation status across human foetal cerebellar development (Figure S2B and S2C). Application of an epigenetic clock algorithm trained on independent foetal brain datasets showed a positive correlation between differentiation of CbO and their predicted epigenetic age (adjusted R-squared: 0.86 and Pearson's correlation coefficient: 0.94, Figure S2D), confirming the progressive maturation of the organoid. Since we observed a strong correlation between DNA methylation profile and progressive maturation of CbO, we next identified genes showing the most variable time-dependent methylation status (VMGs) during CbO or human foetal cerebellar development and grouped them into time-dependent methylation programs by k-means clustering (Figure 2A and S2E). Among the genes showing an increased methylation status during CbO maturation (clusters 1 and 2) we found transcription factors linked to early cerebellum development including *PAX2*, *PAX5* and *PAX6* and to cell lineage specification such as *LMX1A*, *OTX2* and *SOX1*. On the contrary, genes involved in neuronal differentiation and axon-guidance like *MAP2*, *MAP4*, *MAP7* and *GRIP1* were progressively hypomethylated later during CbO differentiation (cluster 4 and 5) (Figure 2A). We found 617 common VMGs between

CbO and human cerebellum and comparative analysis of their methylation level through development, showed the strongest correlation between D35 CbO and 19-20 PCW human cerebellum (Figure 2B). GO analysis of genes included in the identified CbO VMG clusters revealed enrichment for biological processes related to embryogenesis, fate specification and organ development among the early hypomethylated clusters (clusters 1 and 2) while genes showing a later hypomethylation pattern (clusters 4 and 5) were involved in neuronal differentiation, signal transduction and structural functions such as synaptic junctions and neuron projections (Figure 2C). Similar GO pathways including nervous system and organ development, cell adhesion and synaptic junctions were identified from human developmental VMG clusters (Figure S2F). Finally, to explore the impact on gene expression of the observed DNA methylation changes, we integrated DNA methylation and RNA expression analysis to identify genes with concordant methylation status and expression between D7 and D35 (i.e. hypomethylated and upregulated or hypermethylated and downregulated, Figure 2D). We found a significant enrichment for pathways involved in tissue morphogenesis, proliferation and receptor signalling for hypermethylated/downregulated genes expressed during early CbO development and enrichment of neuronal synapse pathways for hypomethylated/upregulated genes expressed later in CbO differentiation (Figure 2E).

All together our data show that the maturation of CbO follows conserved epigenetically regulated CNS developmental pathways and epigenetically date D35 CbO as achieving a differentiation comparable to 19 PCW human cerebellum.

CbO reproduce the spatiotemporal cellular complexity required for medulloblastoma initiation.

Next, we compared the *in vitro* maturation process to human cerebellar development by analysing pseudo-bulk RNA-Seq obtained from CbO against datasets obtained from developing foetal cerebellum [34-36] and found that D35/49 CbO show a high correlation in age-related gene sets with human cerebellum between 17 and 20 PCW (Figure 3A). Interestingly, cerebellar organoids from previous studies [22-24] acquire a similar profile of expression after a longer maturation period (Figure 3A) suggesting a

faster commitment and differentiation of CbO obtained from EPSC relative to those from iPSCs.

Recent seminal studies have described a common rhombic lip (RL) origin for G3 and G4 MB and identified their putative cell-of-origin by analysing human cerebellum between 14 and 19 PCW [14,15], a developmental stage that we model with our CbO. Hence, we compared the methylation profile of CbO and micro-dissected human foetal RL and external granular layer (EGL), the region of origin of SHH MB, and we found a marked increase in correlation during CbO differentiation with RL as compared to EGL (Figure 3B). G3/G4 MB cells-of-origin are thought to be developmentally restricted to the RL subventricular zone (RL^{SVZ}) [14,15]. We confirmed enrichment for a RL^{SVZ} expression signature in glutamatergic-related cell clusters (Figure 3C), further suggesting that upon differentiation the CbO display a cell complexity in keeping with the region G3/G4 MB are thought to originate. Previous studies showed enrichment of photoreceptor and UBC expression signatures in RL^{SVZ}, with a high expression in G3 and G4 MB respectively. Quantification of photoreceptor and UBC signatures within CbO trajectories confirmed their enrichment at the discrete clusters of eCN and glutamatergic neuron progenitors respectively (Figure 3D and S3A). A specific enrichment for G3 and G4 MB-derived signatures [55] (Figure S3B) and mutually exclusive expression of OTX2 or CBFA complex, previously described as showing a MB subtype-specific profile (Figure S3C) [15], were also observed in eCN and glutamatergic neuron progenitors. We next turned to computational lineage tracing methods to further investigate the putative progenitor populations. RNAvelocity vector fields revealed two independent unidirectional streams connecting eCN and glutamatergic progenitors to more mature neuronal populations (Figure S3D). We therefore calculated pseudotime independently over the G3 (via eCN progenitors) and G4 (via glutamatergic neuron progenitors) trajectories (Figure S3E). This revealed both shared (*SOX2*, *EOMES*) and cell lineage-specific changes in gene expression over pseudotime for cells in the G3 (*OTX2*, *NEUROG1* and *ONECUT1*) and G4 (*NPTX2*, *OLIG1*) trajectories (Figure S3F,G). Importantly, we observed $EOMES^{+}KI76^{+}$ cells in our CbO, reminiscent of the human-specific MB-susceptible progenitors of G3 and G4 (Figure 3E,F) [55].

Taken together our data show that D35 CbO displays an epigenetic and transcriptional landscape mirroring the cellular composition and cerebellar developmental stage of G3/G4 MBs initiation.

CbO sustain medulloblastoma cells proliferation and invasion while preserving their molecular identity.

Leveraging the observation that CbO mirrors the cellular complexity of human developing cerebellum at the time of G3/G4 MB initiation, we set out to assess whether our CbO could provide a physiologically relevant 3D environment for sustaining growth of human MB cells. We co-cultured three independent GFP-tagged G3/G4 MB lines (ICb1299, CHLA-10-Med, CHLA-01R-Med) with D35 CbO (Figure 4A). All the tested MB lines successfully attached and infiltrated the CbO with considerable cell growth after 14 days of co-culture (Figure 4A and S4A). Morphological analysis of CbO bearing MB cells (CbO-MB) showed a highly cellular and proliferative pleomorphic tumour, in keeping with MB, diffusely infiltrating the adjacent CbO tissue (Figure S4B). We observed positivity for the proliferation marker Ki-67 in around 30% of GFP^+ MB cells (Figure 4B), thus confirming that CbO can sustain MB cells proliferation and infiltration.

To explore the effect of MB cells on CbO, we performed scRNA-Seq on 10,000 cells from a pool of 5 CbO-MB after 14 days of co-culture (Figure 4A). Louvain clustering and inferred copy number analysis identified MB cells that represent more than 80% of the CbO-MB cells (Figure 4C and S4C), and cell cycle signature scoring further confirmed MB cell proliferation upon co-culture (Figure S4D). To investigate the degree to which co-cultured CbO-MB cells retained their subtype specificity, we correlated pseudobulk transcriptional profiles of MB co-cultured cells with those from a cohort of patient tumours [37]. As expected, they fell within an intermediate subcluster containing both G3 and G4 primary tumours (Figure 4D). Similarly, when interrogating single cells for patient derived gene signatures, we observed a significant increase in average G3/G4 metaprogram [37] when compared to WNT or SHH scores (Figure 4E), further confirming that MB cells retains their molecular subtype in the CbO-MB model. Studies of glioblastoma have shown that tumour cells more closely recapitulate their parental tumours when co-cultured in brain organoids as compared to 2D models [19].

We therefore correlated expression profiles of the same MB cells co-cultured with CbO or in 2D with patient tumour samples [28,37] . Importantly, we observed a significantly higher correlation in co-cultured MB cells (Figure 4F), suggesting that CbO-MB better phenocopies the *in vivo* primary tumours.

These data show that CbO represents a novel 3D model for MB cells growth and expansion which is superior at preserving the MB subgroup's molecular profile as compared to 2D cultures.

CbO-MB reveals a differential impact of medulloblastoma engraftment on the cells of the tumour microenvironment.

Little is known about the MB tumour microenvironment (TME), both in terms of the crosstalk between MB cells and non-neoplastic neuronal lineages and the molecular regulators of this interaction, or about the contribution of the MB-TME interplay to treatment response and recurrence in patients [56]. To investigate how MB cells affect CbO cellular complexity, we identified CbO-specific cell types in CbO-MB using our non-co-cultured organoid as reference. The obtained joint cell clusters were then annotated based on their cell composition (Figure 5A and S5A). Upon MB co-culture, we observed a dramatic decrease in the percentage of cycling and hindbrain stem cells, glutamatergic neuron progenitors and mature neurons, both glutamatergic and Purkinje/GABAergic (Figure 5A), suggesting a selective negative effect mediated by MB cells on the viability of these populations. By contrast, the percentage of GPC, ependymal, roof plate/RL NSC and NSC cells were increased in CbO-MB indicating that these cell types might be more resistant to the addition of MB cells (Figure 5A). To characterise the molecular events driving the MB-TME crosstalk we applied a receptor-ligand model using CellphoneDB (Figure S5B). We observed interactions of MB cells with decreased CbO cell types mainly mediated by the cell adhesion proteins CADM1 and CADM3, the NOTCH signalling pathway, the receptor NRP2 and the metallopeptidase inhibitor TIMP1 (Figure 5B). To gain further insights into the effect of MB cells on the surrounding CNS tissue, we investigated cell type-specific transcriptional modulation caused by the presence of MB cells and identified differentially expressed genes (DEG) (Figure S5C) in cell types showing increased or decreased percentage upon MB co-culture. Gene lists were subsequently interrogated

via pathway analysis on deregulated genes within grouped populations based on their differentiation state and effect of MB co-culture on population size. Interestingly, we found selective enrichment for G2/M and G1/S phases of the cell cycle in the cycling stem cells (Figure 5C) as well as enrichment for cell stress related pathways and for respiratory electron transport in Mature Glutamatergic Neurons, possibly explaining their decreased percentage upon MB co-culture (Figure 5D). On the contrary, pathways related to proteins translation and aminoacidic metabolism were enriched among the upregulated genes in all cell populations which increased upon MB co-culture (Figure 5E,F), with neuronal specific axon-guidance pathways in more differentiated GPC/ependymal cells (Figure 5F), suggesting that these cells better tolerate MB co-culture albeit in a more stressed state.

Our data show that CbO-MB is a 3D model suitable for studying cell-cell interactions and molecular events/cascades induced by MB cells engraftment and identified specific populations of CNS tissue that are more exposed to detrimental stimuli during MB formation and expansion.

CbO-MB are a novel and effective pre-clinical drug testing tool.

Following on from the observations that CbO-MB maintain tumour cells in a molecular state closer to the human samples whilst simultaneously providing insights into the functional impact of MB growth on the surrounding cerebellum, we sought to investigate whether CbO-MB could be suitable as a drug testing tool. We previously demonstrated that combination therapy with BMI1 (PTC-209) and MAPK (PD325901) inhibitors or the phospho-inositol metabolic modulator IP6 extends survival of mice xenografted with MB cells recapitulating a specific molecular signature found in a proportion of MB tumours, whereby the PcG gene BMI1 and the chromatin remodelling factor CHD7 are overexpressed and downregulated respectively ($BMI1^{High}$;$CHD7^{Low}$) [28,57]. Here, we co-cultured GFP-tagged $BMI1^{High}$;$CHD7^{Low}$ MB cells with D35 CbO and treated CbO-MB at 14 days, a timepoint when a large population of proliferative MB cells was established (Figure 4B), with BMI1/MAPK inhibitors or IP6 for four days (Figure 5G). We observed a significant decrease of GFP^{+} $BMI1^{High}$;$CHD7^{Low}$ MB cells upon both treatments, with no significant impact on CbO cells (Figure 5H,I and Figure S5D,E), confirming that MB cells grown in these 3D models recapitulate the treatment

response as observed in a widely accepted pre-clinical *in vivo* model, whilst also indicating negligible side effects on CbO-MB non-neoplastic cells.

Taken together, these data show that CbO-MB are an effective 3D *in vitro* drug testing tool which perform similarly to *in vivo* xenograft models.

Discussion

We describe a novel EPSC-derived cerebellar organoid (CbO) model which faithfully recapitulates the developmental stages of the human cerebellum essential for MB initiation. Epigenetic and single cell transcriptomic profiling of this CbO model demonstrates cell lineages displaying gene signatures enriched in G3 and G4 MB cell-of-origin. Moreover, co-culture of patient-derived MB cells within the CbO generates a 3D *in vitro* model which sustains MB cells proliferation and invasion while preserving their molecular identity and recapitulates the results obtained in pre-clinical *in vivo* drug testing.

Recent studies have shown the fundamental role of human-specific progenitor cells residing in RL^{SVZ} in the development of G3 and G4 MB [14,15], clearly exposing the limitations of mouse models particularly for G4 MB and highlighting the need for new human-specific models. The G3 and G4 MB cell-of-origin are generated in RL^{SVZ} upon RL compartmentalisation at 11 PCW and show a specific spatiotemporal pattern that peaks at around 14-19 PCW. Previously published cerebellar organoid protocols observed a correlation between 2 months-old organoid cell populations and RL cell clusters from human datasets [24] and a modest enrichment for UBC signature in GNPs cluster of a 3-months old organoid [14]. Here, we leveraged comparative epigenetic and transcriptomic analysis of our CbO model and human cerebellar tissue samples to accurately characterise and date the development of our model and provide the first compelling evidence that it faithfully recapitulates stages of human development known to enable MB initiation. We observed a significant enrichment for RL^{SVZ} signatures in discrete cell clusters of a 1-month-old organoid. Importantly, we identified specific cell clusters showing enrichment for UBC and photoreceptor expression signatures, the latter never observed before in previous organoid models. Strikingly, we found $EOMES^{+}KI67^{+}$ cells in D35 CbO recapitulating the human-specific progenitors susceptible to neoplastic transformation in the developing cerebellum. Interestingly, our CbO model achieves the relevant developmental stage at an earlier timepoint as compared to other cerebellar organoid studies. The totipotent characteristics of EPSCs that we used to generate CbO appear to be advantageous for prompt and reproducible cerebellar commitment and differentiation as compared to iPSC-derived organoids, where line-dependent heterogeneity has also been observed [22,58]. Importantly, the earlier commitment and differentiation obtained in this

study, with specific human MB cell-of-origin appearing in early stages of CbO differentiation, represents a major improvement for tumour initiation studies giving access to tumour-susceptible progenitors in a 3D model whilst degenerative changes linked to protracted culturing such as necrosis and hypoxia are still relatively mild. Therefore, our CbO model provides an unparalleled opportunity for modelling the initiation of G3 and G4 MB by providing access to their human-specific cell-of-origin in a 3D experimental system.

In vitro growth of MB cells isolated from patients tissue has proven difficult particularly for G4, thus the number of reliable MB cell lines for use in 2D *in vitro* cell culture or PDX assays is limited [8,9]. Moreover, *in vitro* expansion can lead to shifts in molecular subgrouping, an issue that is particularly relevant for G3/G4 MB [4,59]. We successfully co-cultured multiple G3/G4 MB cell lines with CbO showing that our 3D co-culture model represents a valuable tool to grow and maintain primary MB cell lines for which the 2D culture has proven challenging by exposing tumour cells to cell-extrinsic signals from the adjacent CNS tissue. Importantly, we observed for the first time that MB cells in the 3D CbO-MB model retain an expression profile closer to that of patient tumours as compared to 2D cultures suggesting that the CbO environment is superior in supporting and preserving the molecular identity of MB cells, as has been demonstrated in co-culture models for other brain tumours [60]. Of note, despite G3/G4 MB typically manifesting themselves post-natally, cases of congenital MB have been reported [61,62], suggesting that the pre-natal cerebellum which we model in CbO is a permissive ecosystem for MB formation, proliferation and invasion. While multiple studies have reported the successful co-culture of primary adult glioblastoma cells with cerebral organoids [18,19], this is the first time that this approach has been successfully applied to MB cells.

Co-culture models have been successfully applied to identify TME components and interactions in other primary and metastatic brain tumours [63,64], although the network between MB and cerebellar cells and their role in promoting tumour growth while potentially impacting specific cerebellar cell populations is still rather unexplored. Our human CbO offers the opportunity to characterise the interplay between MB and cerebellar cells of neuroectodermal origin, hence enabling studies into the contribution of the TME to MB progression, drug response and recurrence. We observed a reduction in cell populations that arise earlier in the CbO development, such as cycling

stem cells and hindbrain stem cells, which demonstrated an impact on pathways involved in stages of the cell cycle, the balance of which has been shown to affect cell fate decisions [65]. A scenario whereby these populations are induced to differentiate upon MB co-culture is therefore conceivable, potentially explaining the subsequent increase in more differentiated cell populations including GPC, ependymal and choroid plexus-like cells and NSCs observed. Neurons can produce several mitogenic signals within the brain to sustain NSC growth [66] and neuronal activity can promote high-grade gliomas progression [67-69], however very little is known about the interplay between MB cells and neurons. We observed that upon MB co-culture both Purkinje/GABA neurons and mature glutamatergic neurons were dramatically decreased. In particular we observed interactions between MB cells and these populations of neurons mediated by the cell adhesion protein CADM3, an extracellular matrix component modulated in MB which is associated to cellular invasion and migration in glioma [70], and the transmembrane protein NRP2 (Neuropilin-2), previously linked to cell proliferation in a MB mouse model [71]. We also observed interaction with the surrounding cerebellar cells via NOTCH signalling, with MB cells specifically expressing DLL1 and DLL3 ligands previously described to be involved in MB's prognosis, tumour microenvironment and metastasis [72,73]. Interestingly, we also found interactions mediated by the cytokine TIMP1 (Tissue Inhibitor of Metallo Proteinase 1) whose expression in CSF correlates with metastatic G3 MB [74].

Finally, our model recapitulates the therapeutic response upon treatment with BMI1/MAPK inhibitors and IP6 as previously demonstrated in xenograft models, hence supporting its potential value as a system for testing MB subgroup specific and signature-matched therapeutic approaches. Notably, Cbo-MB model is faster, scalable and more cost-effective as compared to expansion of MB cells in immunodeficient mice, whilst also offering the possibility to evaluate toxicity on cerebellar cells induced by anti-tumour therapy, hence could be used in precision medicine modelling to identify new treatment options that are still lacking for G3/G4 patients.

In conclusion, we have established a new human cerebellar organoid system that offers unparalleled opportunities to study MB pathogenesis by providing (i) access to human MB cell-of-origin to understand tumour initiation, (ii) a human-specific 3D model

of the tumour microenvironment to study the interaction between MB and cerebellar cells and (iii) a novel scalable pre-clinical screening platform for precision medicine.

Acknowledgements

This work is funded by grants from Brain Tumour Research (Centre of Excellence award to S.M.), Cancer Research UK (C23985/A29199 programme award to S.M.), Barts Charity (MGU0447 programme grant to S.M.). We thank Gary Warnes (Blizard Flow Cytometry Core Facility), Maeve McLaughlin (Blizard Advanced Light Microscopy Facility), Imran Uddin (Single Cell Genomics Facility, UCL, Cancer Institute), Myrianni Constantinou and Sara Lucchini for sharing their expertise. We thank Massimo Ganassi for support in the preparation of the figures. The collection and annotation of human tissue samples is funded by the NIHR GOSH BRC.

Author contribution

SB and SM conceived and supervised the project; TW, SB and SM designed the experiments; TW performed, analysed and interpreted all experiments and data; SB analysed and interpreted all experiments and data; JN analysed and interpreted scRNA-seq data; TW and YX analysed DNA methylation data; OO, TM and AM identified and provided suitable human foetal cerebellar samples; NRZ contributed essential expertise to DNA methylation analysis; SM secured financial support; TW, SB and SM wrote the paper with contributions from all authors.

Declaration of interests

The authors declare no competing interests for this study.

Data Availability

The authors declare that all the data supporting the findings of this study are available within the article and its supplementary files. The scRNA-seq and DNA methylation datasets generated in this study and processed data are available in the NCBI Gene Expression Omnibus database (GSE263652 and GSE263653 respectively) or are available from the corresponding authors upon reasonable request. Publicly available datasets used in the study were retrieved from relevant databases as outlined in materials and methods.

Code Availability

The authors declare that no custom code was used in this study. A full description of analyses including functions and packages used are stated in the materials and methods. Specific code will be made available from the corresponding authors upon reasonable request.

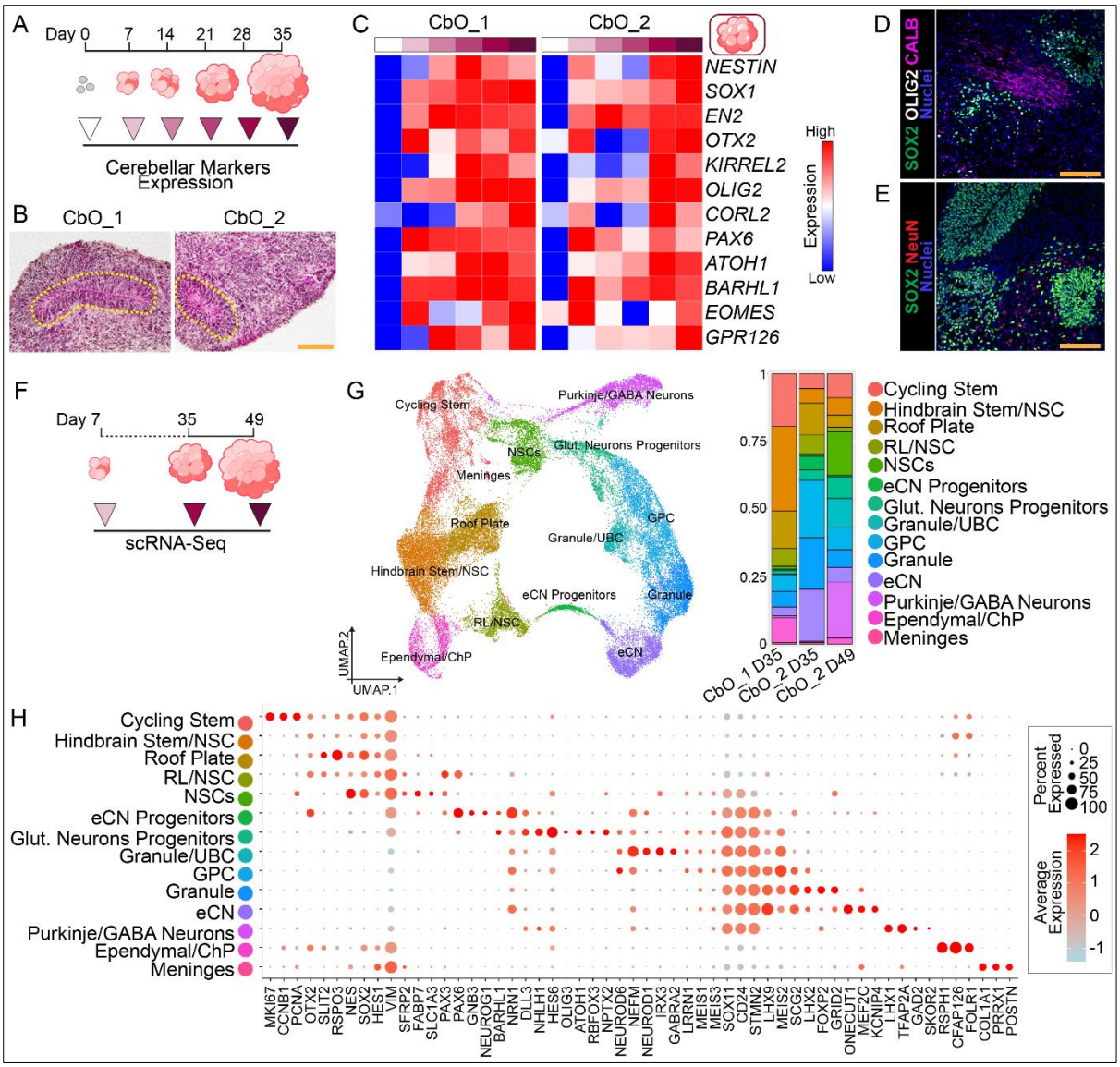

Figure 1. CbO is composed of diverse cerebellar lineages and displays characteristic structural organisation.

A. Schematic of CbO samples used to assess expression of cerebellar markers.

B. H&E staining of CbO showing formation of characteristic flat-oval neural rosettes.

C. Heatmaps showing average expression of marker genes associated with cerebellar differentiation across development of CbO_1 and CbO_2 derived from two independent EPSC lines. n = 3 independent CbO per timepoint.

D. Representative immunofluorescence staining of OLIG2^{+} GABAergic progenitors (white), Calbindin^{+} (CALB^{+}) mature neurons (pink) and SOX2^{+} neural stem and progenitor cells (green).

E. Representative immunofluorescence staining of NeuN^{+} glutamatergic neuronal cells (red) and SOX2^{+} neural stem and progenitor cells (green).

F. Schematic of CbO samples used in single cell RNA-Seq (scRNA-Seq) analysis.
G. Uniform manifold approximation and projection (UMAP) plot of scRNA-Seq data from CbO (CbO_1 and CbO_2) at Day 35 (D35) and Day 49 (D49) of differentiation (left) and bar plots showing percentages of cell populations identified (right).
H. Dot plot showing key marker genes used to identify major cell types in CbO (see also Figure S1J).

Scale bars = 150 µm (B) and 100 µm (D and E).

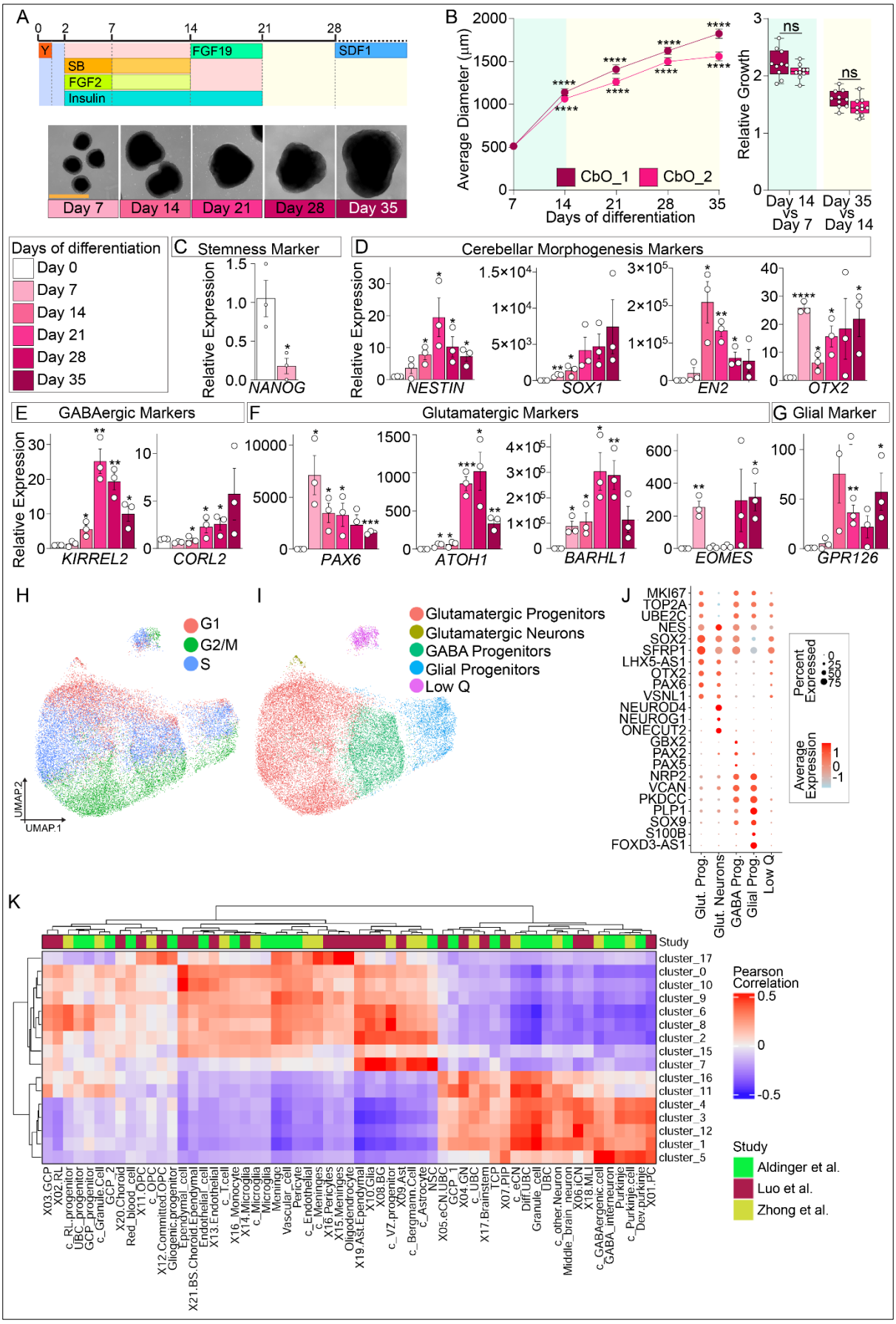
A
Y
SB
FGF2
Insulin
FGF19
SDF1
Day 7
Day 14
Day 21
Day 28
Day 35
B
Average Diameter (µm)
Days of differentiation
CbO_1
CbO_2
Relative Growth
ns
Day 14 vs Day 7
Day 35 vs Day 14
Days of differentiation
Day 0
Day 7
Day 14
Day 21
Day 28
Day 35
C Stemness Marker
Relative Expression
NANOG
D Cerebellar Morphogenesis Markers
NESTIN
SOX1
EN2
OTX2
E GABAergic Markers
KIRREL2
CORL2
F Glutamatergic Markers
PAX6
ATOH1
BARHL1
EOMES
G Glial Marker
GPR126
H
G1
G2/M
S
UMAP.2
UMAP.1
I
Glutamatergic Progenitors
Glutamatergic Neurons
GABA Progenitors
Glial Progenitors
Low Q
J
MKI67
TOP2A
UBE2C
NES
SOX2
SFRP1
LHX5-AS1
OTX2
PAX6
VSNL1
NEUROD4
NEUROG1
ONECUT2
GBX2
PAX2
PAX5
NRP2
VCAN
PKDCC
PLP1
SOX9
S100B
FOXD3-AS1
Glut. Prog.
Glut. Neurons
GABA Prog.
Glial Prog.
Low Q
Percent Expressed
Average Expression
K
Study
cluster_17
cluster_0
cluster_10
cluster_9
cluster_6
cluster_8
cluster_2
cluster_15
cluster_7
cluster_16
cluster_11
cluster_4
cluster_3
cluster_12
cluster_1
cluster_5
Pearson Correlation
Study
Aldinger et al.
Luo et al.
Zhong et al.

Supplementary Figure 1. CbO displays sustained growth and maturation.

A. Schematic of protocol used to generate and differentiate CbO, (see Methods, Y: Y-27632 Dihydrochloride and SB: SB431542) and representative brightfield pictures of CbO upon 7, 14, 21, 28 and 35 days of differentiation. Scale bar = 1000 µm.
B. Diameter analysis of CbO obtained from two independent EPSC lines (CbO_1 and CbO_2) across 35 days of maturation (left) and analysis of relative growth comparing Day 14 to Day 7 or Day 35. Asterisks indicate p-values between given time point and Day 7, two-way ANOVA, ns: not significant. n = 10 independent CbO average diameters per timepoint.
C. qPCR analysis showing quantification of *NANOG* expression in CbO across 35 days of maturation.
D. qPCR analysis showing quantification of *NESTIN, SOX1, EN2* and *OTX2* expression in CbO across 35 days of maturation.
E. qPCR analysis showing quantification of *KIRREL2* and *CORL2* expression in CbO across 35 days of maturation.
F. qPCR analysis showing quantification of *PAX6, ATOH1, BARHL1* and *EOMES* expression in CbO across 35 days of maturation.
G. qPCR analysis showing quantification of *GPR126* expression in CbO across 35 days of maturation.
H. UMAP plot of scRNA-Seq data from CbO at Day 7 of differentiation coloured by cell cycle phases.
I. UMAP plot of scRNA-Seq data from CbO at Day 7 of differentiation coloured by annotated Louvain clusters.
J. Dot plot showing key marker genes used to identify major cell types in CbO at Day 7 of differentiation.
K. Heatmap showing correlation of clusters identified in Figure 2B and cell populations of human developing cerebellum from reference human foetal tissue.

All graphs report mean ± SEM, unpaired t-test. n = 3 independent CbO per timepoint.

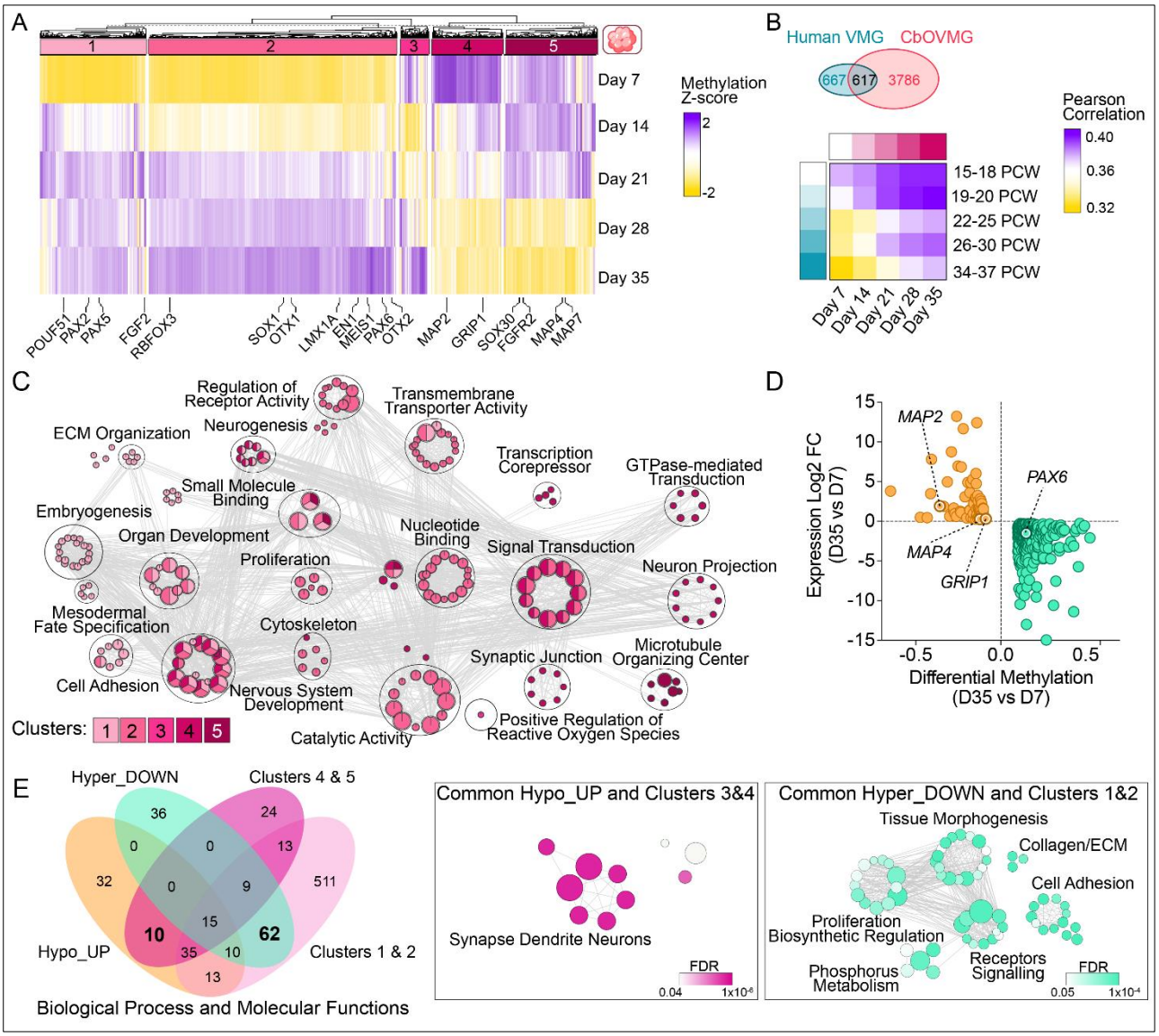

Figure 2. CbO development is epigenetically regulated similarly to human cerebellum.

A. Heatmap showing clustering of most variable methylated genes across 35 days of CbO maturation based on z-score of methylation level.

B. Venn diagram showing common variable methylated genes (VMGs) identified across human foetal cerebellar development (Human VMG) and CbO (CbO VMG) (top panel). Heatmap showing correlation between differentiation of CbO and development of human cerebellum based on the methylation level of 617 common VMGs (bottom panel).

C. Bubble plot showing top 100 significant (adjusted p-value < 0.05) GO Biological Processes and Molecular Functions of genes from clusters showed in A. Bubbles

are coloured based on specific clusters and size is proportional to number of genes in specific GO term.

D. Volcano plots of differentially expressed (DEG) and differentially methylated (DMG) genes between D35 and D7 of CbO maturation. Orange and green dots represent upregulated/hypomethylated and downregulated/hypermethylated genes respectively. Genes found in VMG clusters in A are highlighted.

E. Venn diagram showing integrative analysis of significant GOs in most variable methylated (from A) and concordant (from E) genes (left panel). Bubbles plot showing 10 common pathways between genes upregulated/hypomethylated and in clusters 3 and 4 (middle panel) or genes downregulated/hypermethylated and in clusters 1 and 2 (left panel). Bubbles are coloured based on FDR and size is proportional to number of genes of specific GO term.

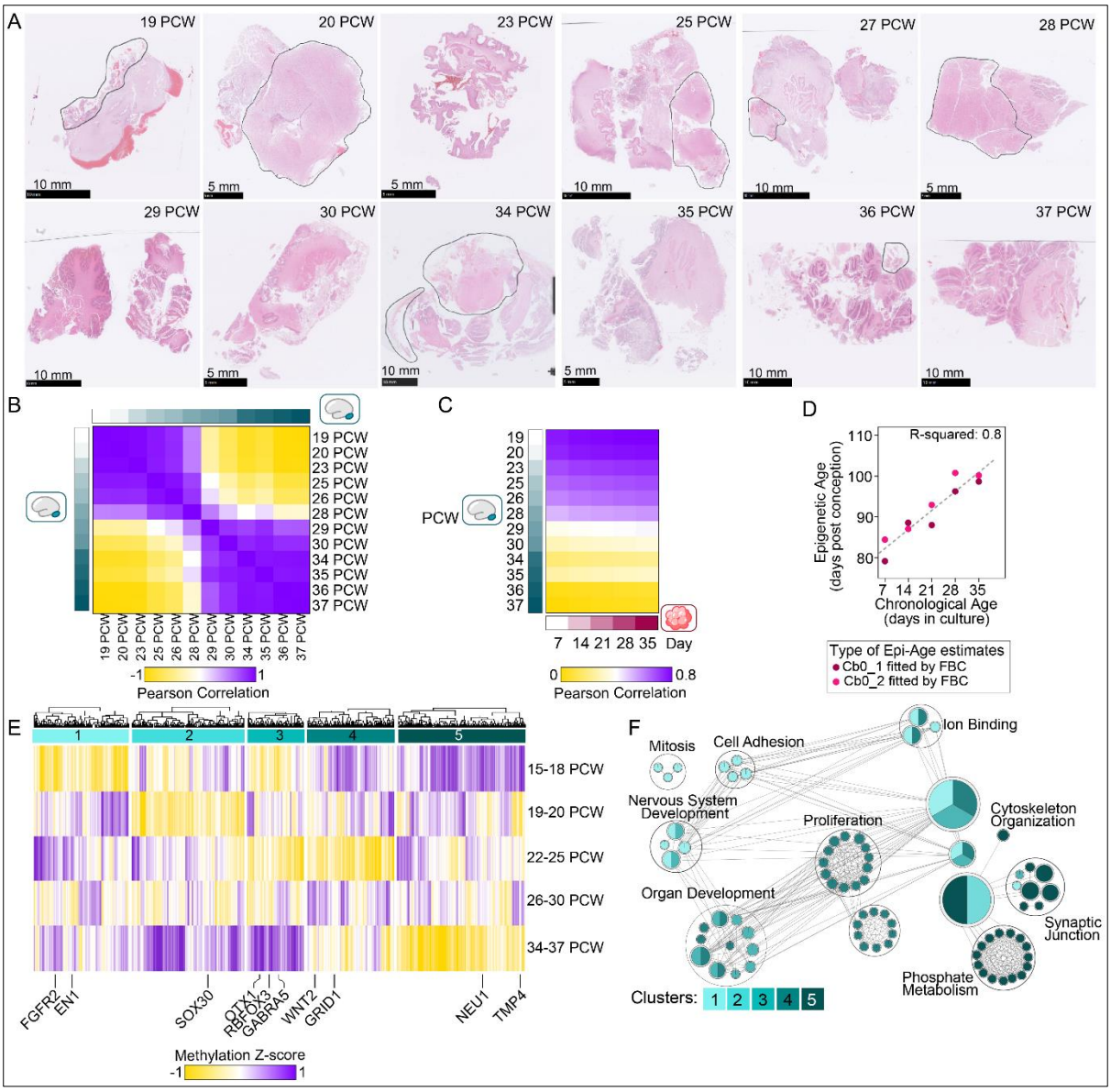

Supplementary Figure 2. Staging development of CbO comparatively to human cerebellum reveals conserved epigenetically regulated genes and pathways.

A. H&E staining of FFPE samples from human foetal cerebellum. Non-cerebellar tissue excluded from the microdissection is circled. Developmental stage and scale bars are shown.
B. Heatmap showing correlation of methylation status of top 1% age-dependent probes between human developing cerebellum samples.
C. Heatmap showing correlation of methylation status of top 1% age-dependent probes (as in B) between developing human cerebellum and CbO across 35 days of differentiation.
D. Correlation plot between days of maturation of the CbO (chronological age) and the modelled epigenetic ages from the foetal brain clock.

E. Heatmap showing clustering of most variable methylated genes across human foetal cerebellar development based on z-score of methylation level.

F. Bubble plot showing significant (adjusted p-value < 0.05) GO Biological Processes and Molecular Functions of genes from clusters shown in E. Bubbles are coloured based on specific cluster and size is proportional to number of genes in specific GO term.

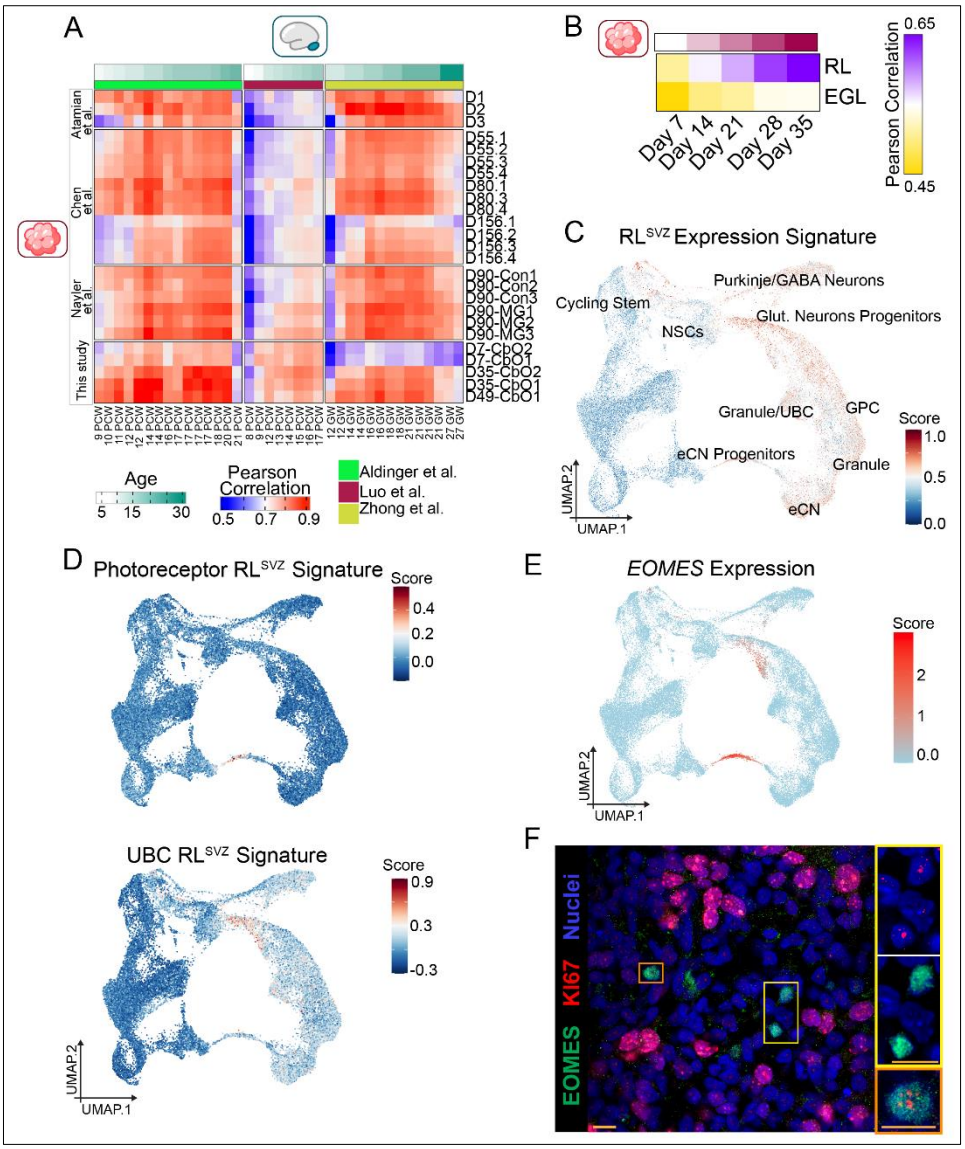

Figure 3. CbO displays spatiotemporal expression of G3/G4 MB cell-of-origin.

A. Heatmap showing correlation of age-related gene sets between expression of pseudo-bulk RNA-Seq of CbO and cerebellar organoid from previously published protocols and human foetal cerebellar samples.

B. Heatmap showing correlation of methylation profiles between human RL and EGL regions and CbO across 35 days of differentiation.

C. UMAP plot of scRNA-Seq data from CbO at Day 35-49 of differentiation, cells coloured by RL^{SVZ} signature score.

D. UMAP plot of scRNA-Seq data from CbO at Day 35-49 of differentiation cells coloured by RL^{SVZ} photoreceptor (top) or RL^{SVZ} UBC signature scores (bottom).

E. UMAP plot of scRNA-Seq data from CbO at Day 35-49 of differentiation, cells coloured by alra-imputed expression of *EOMES*.

F. Representative immunofluorescence staining of EOMES^{+}/Ki67^{+} progenitor cells. Scale bars= 10μm.

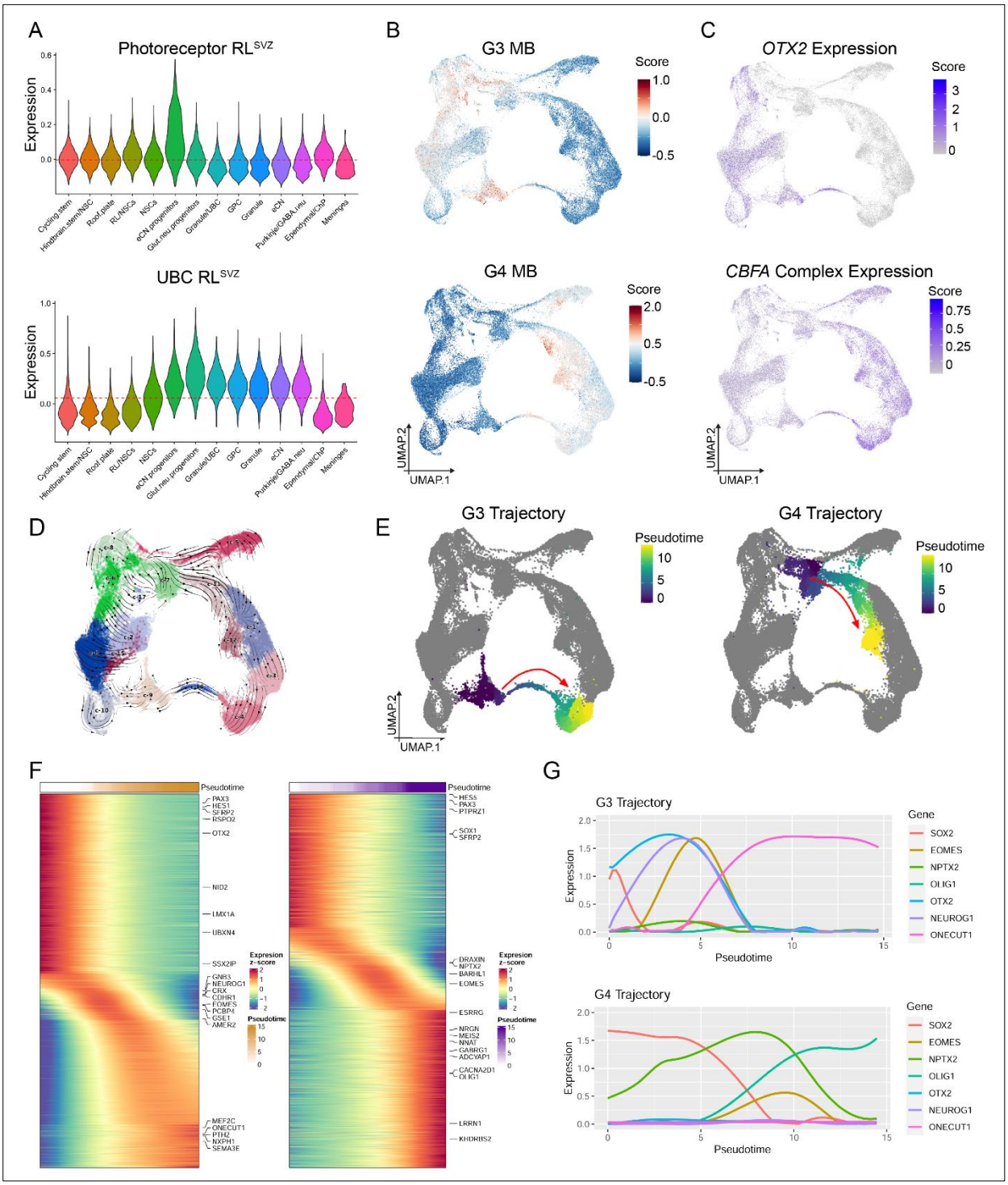

Supplementary Figure 3. CbO clusters harbouring MB cell-of-origin are enriched for distinct G3 and G4 MB associated gene signatures.

A. Violin plots quantifying enrichment of the RL^{SVZ} photoreceptor (top) and RL^{SVZ} UBC (bottom) signatures across cell clusters shown in Figure 3D.

B. UMAP of scRNA-Seq data from CbO at Day 35-49 of differentiation and expression signatures of G3 (top) and G4 (bottom) MB.

C. UMAP of scRNA-Seq data from CbO at Day 35-49 of differentiation and *OTX2* (top) or *CBFA* Complex (bottom) expression.

D. RNA velocity streamlines projected into UMAP embeddings shows two separate unidirectional lineage trajectories in G3 and G4 MB progenitors.

E. UMAP of scRNA-Seq data from CbO at Day 35-49 of differentiation with cells in the G3 (RL/NSCs, eCN Porgenitors, eCN, left) and G4 (NSCs, Glut. Neuron Progenitors, Granule/UBC, right) trajectories coloured by their Pseudotime.

F. Heatmap showing smoothened expression over Pseudotime for the G3 (left) and G4 (right) lineage trajectories.

G. Pseudotime expression plot of marker gene for the G3 (top) and G4 (bottom) lineage.

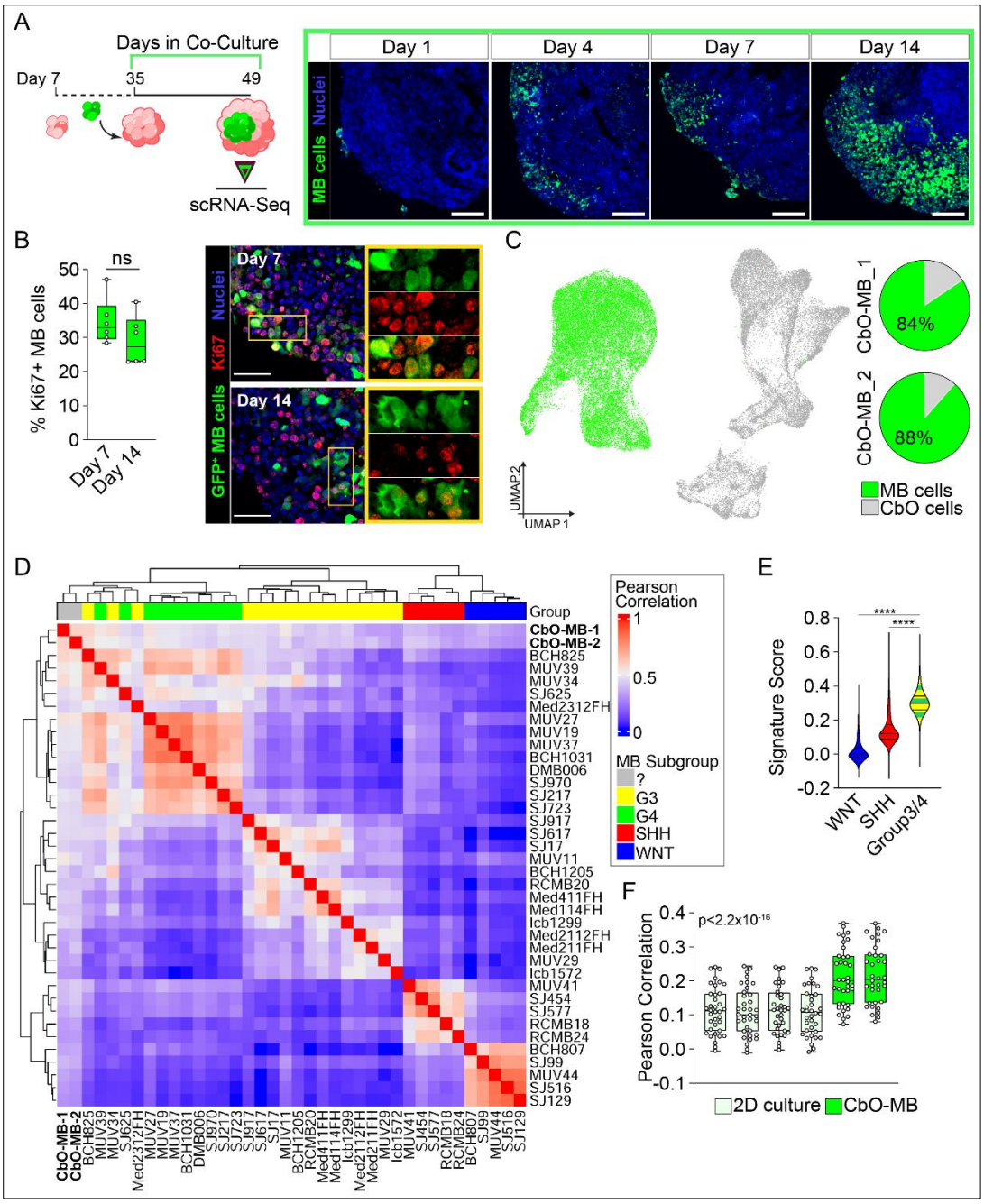

Figure 4. CbO enables MB growth whilst also retaining MB transcriptional profiles closer to those of patient tumour samples.

A. Schematic of protocol used to co-culture CbO with primary MB showing CbO-MB sample used for scRNA-Seq (left panel). Representative immunofluorescence staining of GFP⁺ CHLA-01-Med MB cells upon one, four, seven and fourteen days of co-culture with CbO, scale bars = 100 µm (right panels).

B. Bar plots showing percentage of MB cells (GFP⁺) expressing the proliferative markers Ki67 upon 7 and 14 days of co-culture. Graphs report mean ± SEM, unpaired t-test, n = 6 independent CbO-MB analysed, ns = not significant (left).

Representative immunofluorescence staining of GFP^+ and $KI67^+$ MB cells upon 4 and 14 days of co-culture with CbO, scale bars = 100 µm (right).

C. UMAP plot of scRNA-Seq data from CbO-MB upon 14 days of co-culture (left panel) and pie charts showing percentages of GFP^+ MB cells in two independent CbO-MB (CbO-MB_1 and CbO-MB_2) (right).

D. Heatmap showing correlation scores between expression of pseudo-bulk RNA-Seq of CbO-MB (CbO-MB-1 and CbO-MB-2) and MB samples. Clustering based on expression profile has been used to assess molecular subgroup of CbO-MB models.

E. Violin plot showing signature scores for WNT, SHH or G3/G4 MB subgroups in CbO-MB. One-way ANOVA.

F. Bar plot showing correlations between same MB cell line grown as 2D (light green) or 3D (green) model and MB samples shown in D. One-way ANOVA.

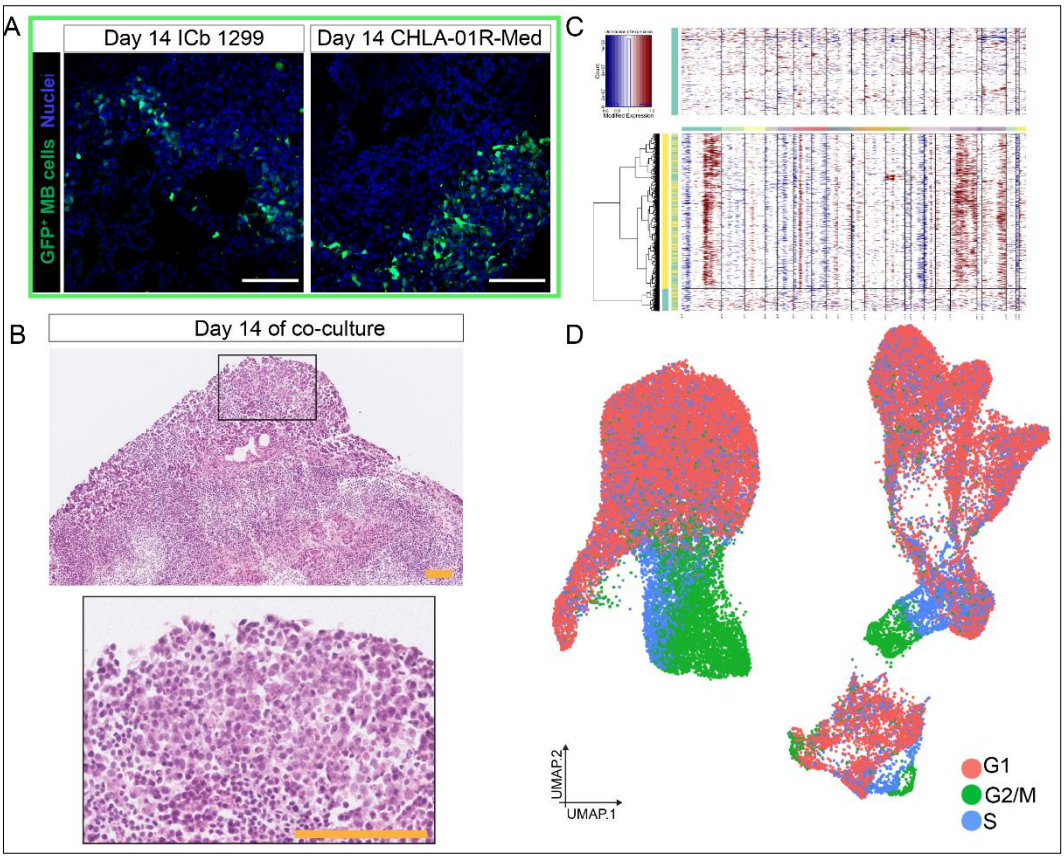

Supplementary Figure 4. MB cells display the morphology of human MB upon co-culture with CbO and retain their genetic features.

A. Representative immunofluorescence staining of two independent GFP+ MB cell lines upon fourteen days of co-culture with CbO, scale bars = 100 µm.
B. H&E stainings of CbO-MB upon 14 days of co-culture with MB cells, scale bars = 100 µm.
C. Hierarchical clustering of inferred copy number profiles separates co-cultured MB and CbO cells.
D. UMAP plot of scRNA-Seq data from CbO-MB upon 14 days of co-culture and annotation of the cell cycle phases.

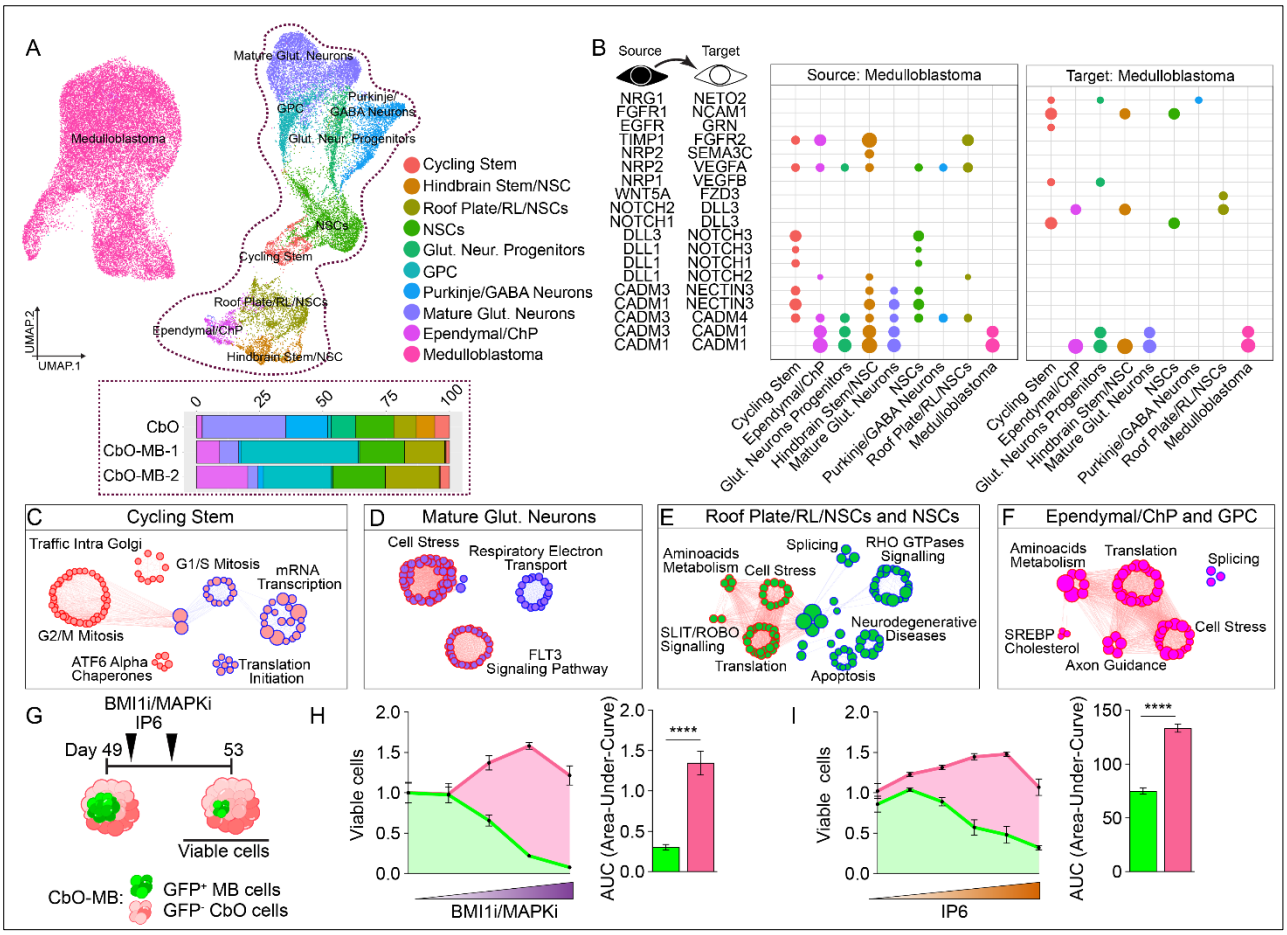

Figure 5. CbO-MB reveal cell-cell interactions and molecular events induced by MB growth and they represent a suitable model for drug screening.

A. UMAP plot of scRNA-Seq data from CbO-MB showing joint cluster annotation (see also Figure S5A) (top). Histograms showing percentages of cell populations (highlighted with dashed lines in UMAP) identified among CbO cells (bottom).

B. Dot plot showing significant receptor-ligand pairs identified by CellPhoneDB analysis used by MB cells as a source (left) or as a target (right) of interaction with reported cell populations of CbO.

C-D. Bubble plot showing top 100 significant Reactome and KEGG Pathways enriched for upregulated (red bubbles and lines) or downregulated (blue bubbles and lines) differentially regulated genes (DEG) in Cycling Stem (C) or Mature Glutamatergic Neurons (D). Bubble size is proportional to number of genes of specific pathway.

E-F. Bubble plot showing top 100 significant Reactome and KEGG Pathways enriched for upregulated (red bubbles and lines) or downregulated (blue bubbles and lines) DEG and in common between Roof Plate/RL/NSCs and NSCs (E) or

Ependymal/ChP and GPC (F). Bubbles size is proportional to number of genes of specific pathway.

G. Schematic of combination treatment with PTC209 (BMI1i) and PD329501 (MAPKi) or IP6 of CbO-MB co-cultures.

H. Viability assays of GFP^+ MB cells (green) and GFP^- CbO cells (pink) upon 4 days of treatment with increasing concentrations of BMI1 and MAPK inhibitors. Measurement of Area Under Curve (AUC) to compare the overall response to treatment. n= 9 independent experiments.

I. Viability assays of GFP^+ MB cells (green) and GFP^- CbO cells (pink) upon 4 days of treatment with increasing concentrations of IP6. Measurement of Area Under Curve (AUC) to compare the overall response to treatment. n= 5 independent experiments

All graphs report mean ± SEM, unpaired t-test.

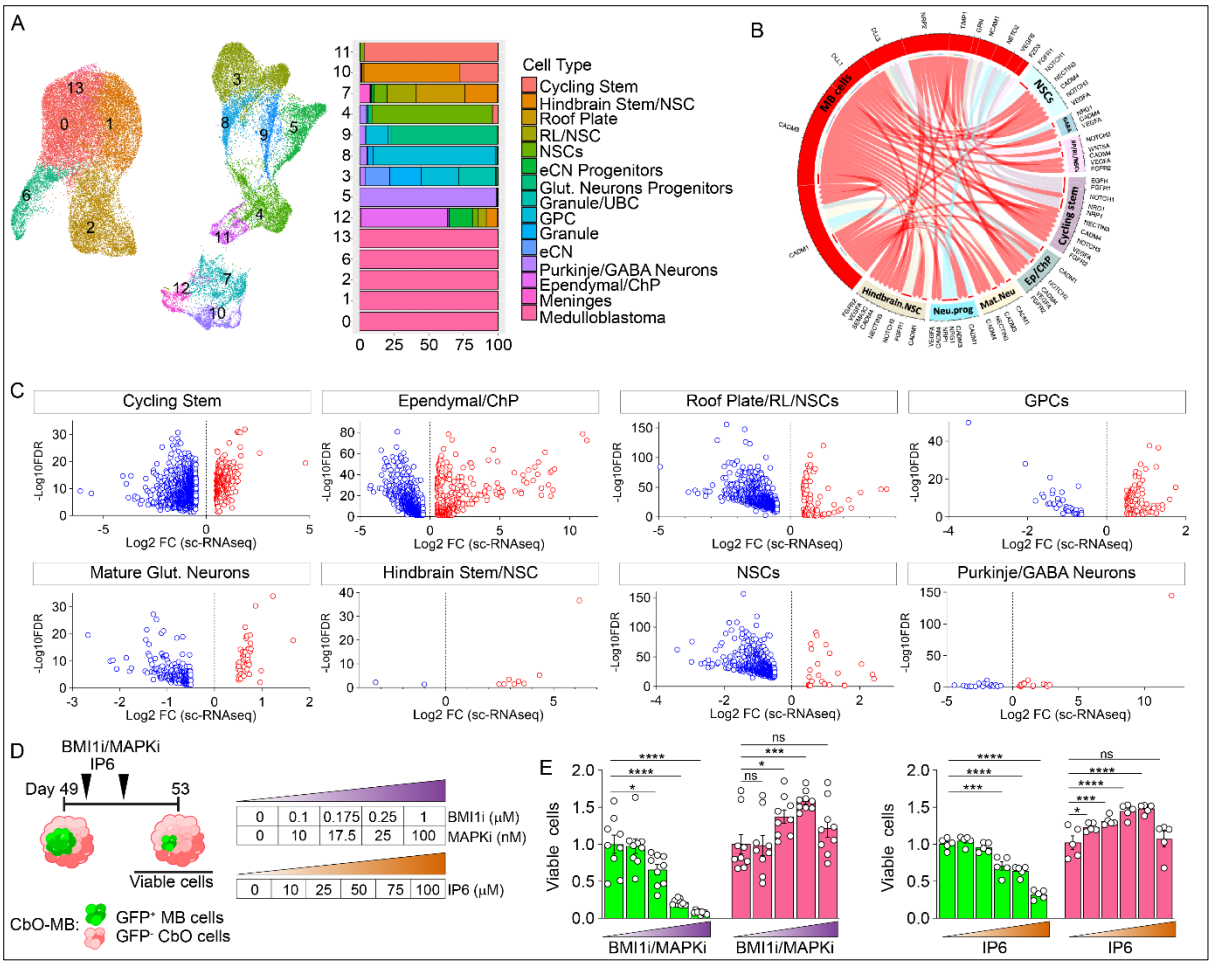

Supplementary Figure 5. Co-culture with MB cells modulates transcriptional profiles of specific CbO lineages.

A. UMAP plot of scRNA-Seq data from CbO-MB showing clusters (left panel) and percentages of cell populations identified in non-treated CbO cells (right panel) used for joint cluster annotation showed in Figure 5A.

B. Circos plot showing significant receptor-ligand pairs identified by CellPhoneDB analysis and represented in Figure 5B.

C. Volcano plots showing significant differentially expressed genes (DEGs) upon MB cells co-culture in indicated cell population. Red and blue dots represent significantly upregulated and downregulated genes respectively.

D. Schematic of CbO-MB treatment with tables reporting the concentrations of PTC209 (BMI1i), PD329501 (MAPKi) and IP6 used.

E. Viability assays of GFP^{+} MB cells (green) and GFP^{-} CbO cells (pink) in CbO-MB upon 4 days of treatment with increasing concentrations of BMI1 and MAPK inhibitors (left) or IP6 (right) as shown in Figure 5H and 5I respectively.

All graphs report mean ± SEM, number of independent CbO analyzed is reported in each graph, one-way ANOVA.

References

1. Cavalli, F.M.G., Remke, M., Rampasek, L., Peacock, J., Shih, D.J.H., Luu, B., Garzia, L., Torchia, J., Nor, C., Morrissy, A.S., et al. (2017). Intertumoral Heterogeneity within Medulloblastoma Subgroups. Cancer Cell *31*, 737-754 e736. 10.1016/j.ccell.2017.05.005.
2. Northcott, P.A., Buchhalter, I., Morrissy, A.S., Hovestadt, V., Weischenfeldt, J., Ehrenberger, T., Grobner, S., Segura-Wang, M., Zichner, T., Rudneva, V.A., et al. (2017). The whole-genome landscape of medulloblastoma subtypes. Nature *547*, 311-317. 10.1038/nature22973.
3. Schwalbe, E.C., Lindsey, J.C., Nakjang, S., Crosier, S., Smith, A.J., Hicks, D., Rafiee, G., Hill, R.M., Iliasova, A., Stone, T., et al. (2017). Novel molecular subgroups for clinical classification and outcome prediction in childhood medulloblastoma: a cohort study. The Lancet Oncology *18*, 958-971. 10.1016/s1470-2045(17)30243-7.
4. Sharma, T., Schwalbe, E.C., Williamson, D., Sill, M., Hovestadt, V., Mynarek, M., Rutkowski, S., Robinson, G.W., Gajjar, A., Cavalli, F., et al. (2019). Second-generation molecular subgrouping of medulloblastoma: an international meta-analysis of Group 3 and Group 4 subtypes. Acta Neuropathol *138*, 309-326. 10.1007/s00401-019-02020-0.
5. Mueller, S., and Chang, S. (2009). Pediatric brain tumors: current treatment strategies and future therapeutic approaches. Neurotherapeutics *6*, 570-586.
6. Rechberger, J.S., Toll, S.A., Vanbilloen, W.J.F., Daniels, D.J., and Khatua, S. (2023). Exploring the Molecular Complexity of Medulloblastoma: Implications for Diagnosis and Treatment. Diagnostics (Basel) *13*. 10.3390/diagnostics13142398.
7. Thompson, E.M., Ashley, D., and Landi, D. (2020). Current medulloblastoma subgroup specific clinical trials. Transl Pediatr *9*, 157-162. 10.21037/tp.2020.03.03.
8. Badodi, S., Marino, S., and Guglielmi, L. (2019). Establishment and Culture of Patient-Derived Primary Medulloblastoma Cell Lines. In Brain Tumor Stem Cells, S. Singh, and C. Venugopal, eds. (Humana Press). https://doi.org/10.1007/978-1-4939-8805-1_3.
9. Ivanov, D.P., Coyle, B., Walker, D.A., and Grabowska, A.M. (2016). In vitro models of medulloblastoma: Choosing the right tool for the job. Journal of Biotechnology *236*, 10-25. 10.1016/j.jbiotec.2016.07.028.
10. Sanden, E., Dyberg, C., Krona, C., Gallo-Oller, G., Olsen, T.K., Enriquez Perez, J., Wickstrom, M., Estekizadeh, A., Kool, M., Visse, E., et al. (2017). Establishment and characterization of an orthotopic patient-derived Group 3 medulloblastoma model for preclinical drug evaluation. Sci Rep *7*, 46366. 10.1038/srep46366.
11. Shu, Q., Wong, K.K., Su, J.M., Adesina, A.M., Yu, L.T., Tsang, Y.T., Antalffy, B.C., Baxter, P., Perlaky, L., Yang, J., et al. (2008). Direct orthotopic transplantation of fresh surgical specimen preserves CD133+ tumor cells in clinically relevant mouse models of medulloblastoma and glioma. Stem Cells *26*, 1414-1424. 10.1634/stemcells.2007-1009.
12. Brabetz, S., Leary, S.E.S., Grobner, S.N., Nakamoto, M.W., Seker-Cin, H., Girard, E.J., Cole, B., Strand, A.D., Bloom, K.L., Hovestadt, V., et al. (2018). A biobank of patient-derived pediatric brain tumor models. Nat Med *24*, 1752-1761. 10.1038/s41591-018-0207-3.

13. Marino, S. (2005). Medulloblastoma: developmental mechanisms out of control. Trends Mol Med *11*, 17-22. 10.1016/j.molmed.2004.11.008.
14. Smith, K.S., Bihannic, L., Gudenas, B.L., Haldipur, P., Tao, R., Gao, Q., Li, Y., Aldinger, K.A., Iskusnykh, I.Y., Chizhikov, V.V., et al. (2022). Unified rhombic lip origins of group 3 and group 4 medulloblastoma. Nature *609*, 1012-1020. 10.1038/s41586-022-05208-9.
15. Hendrikse, L.D., Haldipur, P., Saulnier, O., Millman, J., Sjoboen, A.H., Erickson, A.W., Ong, W., Gordon, V., Coudiere-Morrison, L., Mercier, A.L., et al. (2022). Failure of human rhombic lip differentiation underlies medulloblastoma formation. Nature *609*, 1021-1028. 10.1038/s41586-022-05215-w.
16. Bian, S., Repic, M., Guo, Z., Kavirayani, A., Burkard, T., Bagley, J.A., Krauditsch, C., and Knoblich, J.A. (2018). Genetically engineered cerebral organoids model brain tumor formation. Nat Methods *15*, 631-639. 10.1038/s41592-018-0070-7.
17. Choe, M.S., Kim, J.S., Yeo, H.C., Bae, C.M., Han, H.J., Baek, K., Chang, W., Lim, K.S., Yun, S.P., Shin, I.S., and Lee, M.Y. (2020). A simple metastatic brain cancer model using human embryonic stem cell-derived cerebral organoids. FASEB J *34*, 16464-16475. 10.1096/fj.202000372R.
18. Linkous, A., Balamatsias, D., Snuderl, M., Edwards, L., Miyaguchi, K., Milner, T., Reich, B., Cohen-Gould, L., Storaska, A., Nakayama, Y., et al. (2019). Modeling Patient-Derived Glioblastoma with Cerebral Organoids. Cell Rep *26*, 3203-3211 e3205. 10.1016/j.celrep.2019.02.063.
19. Vinel, C., Rosser, G., Guglielmi, L., Constantinou, M., Pomella, N., Zhang, X., Boot, J.R., Jones, T.A., Millner, T.O., Dumas, A.A., et al. (2021). Comparative epigenetic analysis of tumour initiating cells and syngeneic EPSC-derived neural stem cells in glioblastoma. Nat Commun *12*, 6130. 10.1038/s41467-021-26297-6.
20. Silva, T.P., Bekman, E.P., Fernandes, T.G., Vaz, S.H., Rodrigues, C.A.V., Diogo, M.M., Cabral, J.M.S., and Carmo-Fonseca, M. (2020). Maturation of Human Pluripotent Stem Cell-Derived Cerebellar Neurons in the Absence of Co-culture. Front Bioeng Biotechnol *8*, 70. 10.3389/fbioe.2020.00070.
21. Muguruma, K., Nishiyama, A., Kawakami, H., Hashimoto, K., and Sasai, Y. (2015). Self-organization of polarized cerebellar tissue in 3D culture of human pluripotent stem cells. Cell Rep *10*, 537-550. 10.1016/j.celrep.2014.12.051.
22. Atamian, A., Birtele, M., Hosseini, N., Nguyen, T., Seth, A., Del Dosso, A., Paul, S., Tedeschi, N., Taylor, R., Coba, M.P., et al. (2024). Human cerebellar organoids with functional Purkinje cells. Cell Stem Cell *31*, 39-51 e36. 10.1016/j.stem.2023.11.013.
23. Nayler, S., Agarwal, D., Curion, F., Bowden, R., and Becker, E.B.E. (2021). High-resolution transcriptional landscape of xeno-free human induced pluripotent stem cell-derived cerebellar organoids. Sci Rep *11*, 12959. 10.1038/s41598-021-91846-4.
24. Chen, Y., Bury, L.A., Chen, F., Aldinger, K.A., Miranda, H.C., and Wynshaw-Boris, A. (2023). Generation of advanced cerebellar organoids for neurogenesis and neuronal network development. Hum Mol Genet *32*, 2832-2841. 10.1093/hmg/ddad110.
25. Ballabio, C., Anderle, M., Gianesello, M., Lago, C., Miele, E., Cardano, M., Aiello, G., Piazza, S., Caron, D., Gianno, F., et al. (2020). Modeling medulloblastoma in vivo and with human cerebellar organoids. Nat Commun *11*, 583. 10.1038/s41467-019-13989-3.

26. van Essen, M.J., Apsley, E.J., Riepsaame, J., Xu, R., Northcott, P.A., Cowley, S.A., Jacob, J., and Becker, E.B.E. (2024). PTCH1-mutant human cerebellar organoids exhibit altered neural development and recapitulate early medulloblastoma tumorigenesis. Dis Model Mech *17*. 10.1242/dmm.050323.
27. Zhao, X., Liu, Z., Yu, L., Zhang, Y., Baxter, P., Voicu, H., Gurusiddappa, S., Luan, J., Su, J.M., Leung, H.C., and Li, X.N. (2012). Global gene expression profiling confirms the molecular fidelity of primary tumor-based orthotopic xenograft mouse models of medulloblastoma. Neuro Oncol *14*, 574-583. 10.1093/neuonc/nos061.
28. Badodi, S., Pomella, N., Zhang, X., Rosser, G., Whittingham, J., Niklison-Chirou, M.V., Lim, Y.M., Brandner, S., Morrison, G., Pollard, S.M., et al. (2021). Inositol treatment inhibits medulloblastoma through suppression of epigenetic-driven metabolic adaptation. Nat Commun *12*, 2148. 10.1038/s41467-021-22379-7.
29. Hao, Y., Hao, S., Andersen-Nissen, E., Mauck, W.M., Zheng, S., Butler, A., Lee, M.J., Wilk, A.J., Darby, C., Zager, M., et al. (2021). Integrated analysis of multimodal single-cell data. Cell *184*, 3573-3587.e3529. https://doi.org/10.1016/j.cell.2021.04.048.
30. Korsunsky, I., Millard, N., Fan, J., Slowikowski, K., Zhang, F., Wei, K., Baglaenko, Y., Brenner, M., Loh, P.R., and Raychaudhuri, S. (2019). Fast, sensitive and accurate integration of single-cell data with Harmony. Nat Methods *16*, 1289-1296. 10.1038/s41592-019-0619-0.
31. Finak, G., McDavid, A., Yajima, M., Deng, J., Gersuk, V., Shalek, A.K., Slichter, C.K., Miller, H.W., McElrath, M.J., Prlic, M., et al. (2015). MAST: a flexible statistical framework for assessing transcriptional changes and characterizing heterogeneity in single-cell RNA sequencing data. Genome Biology *16*, 278. 10.1186/s13059-015-0844-5.
32. Bhaduri, A., Andrews, M.G., Mancia Leon, W., Jung, D., Shin, D., Allen, D., Jung, D., Schmunk, G., Haeussler, M., Salma, J., et al. (2020). Cell stress in cortical organoids impairs molecular subtype specification. Nature *578*, 142-148. 10.1038/s41586-020-1962-0.
33. Kanton, S., Boyle, M.J., He, Z., Santel, M., Weigert, A., Sanchis-Calleja, F., Guijarro, P., Sidow, L., Fleck, J.S., Han, D., et al. (2019). Organoid single-cell genomic atlas uncovers human-specific features of brain development. Nature *574*, 418-422. 10.1038/s41586-019-1654-9.
34. Aldinger, K.A., Thomson, Z., Phelps, I.G., Haldipur, P., Deng, M., Timms, A.E., Hirano, M., Santpere, G., Roco, C., Rosenberg, A.B., et al. (2021). Spatial and cell type transcriptional landscape of human cerebellar development. Nat Neurosci *24*, 1163-1175. 10.1038/s41593-021-00872-y.
35. Luo, Z., Xia, M., Shi, W., Zhao, C., Wang, J., Xin, D., Dong, X., Xiong, Y., Zhang, F., Berry, K., et al. (2022). Human fetal cerebellar cell atlas informs medulloblastoma origin and oncogenesis. Nature *612*, 787-794. 10.1038/s41586-022-05487-2.
36. Zhong, S., Wang, M., Huang, L., Chen, Y., Ge, Y., Zhang, J., Shi, Y., Dong, H., Zhou, X., Wang, B., et al. (2023). Single-cell epigenomics and spatiotemporal transcriptomics reveal human cerebellar development. Nat Commun *14*, 7613. 10.1038/s41467-023-43568-6.
37. Hovestadt, V., Smith, K.S., Bihannic, L., Filbin, M.G., Shaw, M.L., Baumgartner, A., DeWitt, J.C., Groves, A., Mayr, L., Weisman, H.R., et al. (2019). Resolving

medulloblastoma cellular architecture by single-cell genomics. Nature *572*, 74-79. 10.1038/s41586-019-1434-6.

38. Venteicher, A.S., Tirosh, I., Hebert, C., Yizhak, K., Neftel, C., Filbin, M.G., Hovestadt, V., Escalante, L.E., Shaw, M.L., Rodman, C., et al. (2017). Decoupling genetics, lineages, and microenvironment in IDH-mutant gliomas by single-cell RNA-seq. Science *355*, eaai8478. doi:10.1126/science.aai8478.
39. La Manno, G., Soldatov, R., Zeisel, A., Braun, E., Hochgerner, H., Petukhov, V., Lidschreiber, K., Kastriti, M.E., Lönnerberg, P., Furlan, A., et al. (2018). RNA velocity of single cells. Nature *560*, 494-498. 10.1038/s41586-018-0414-6.
40. Bergen, V., Lange, M., Peidli, S., Wolf, F.A., and Theis, F.J. (2020). Generalizing RNA velocity to transient cell states through dynamical modeling. Nature Biotechnology *38*, 1408-1414. 10.1038/s41587-020-0591-3.
41. Cao, J., Spielmann, M., Qiu, X., Huang, X., Ibrahim, D.M., Hill, A.J., Zhang, F., Mundlos, S., Christiansen, L., Steemers, F.J., et al. (2019). The single-cell transcriptional landscape of mammalian organogenesis. Nature *566*, 496-502. 10.1038/s41586-019-0969-x.
42. Linderman, G.C., Zhao, J., Roulis, M., Bielecki, P., Flavell, R.A., Nadler, B., and Kluger, Y. (2022). Zero-preserving imputation of single-cell RNA-seq data. Nat Commun *13*, 192. 10.1038/s41467-021-27729-z.
43. Efremova, M., Vento-Tormo, M., Teichmann, S.A., and Vento-Tormo, R. (2020). CellPhoneDB: inferring cell-cell communication from combined expression of multi-subunit ligand-receptor complexes. Nat Protoc *15*, 1484-1506. 10.1038/s41596-020-0292-x.
44. Pidsley, R., Wong, C.C.Y., Volta, M., Lunnon, K., Mill, J., and Schalkwyk, L.C. (2013). A data-driven approach to preprocessing Illumina 450K methylation array data. BMC Genomics *14*. https://doi.org/10.1186/1471-2164-14-293.
45. Steg, L.C., Shireby, G.L., Imm, J., Davies, J.P., Franklin, A., Flynn, R., Namboori, S.C., Bhinge, A., Jeffries, A.R., Burrage, J., et al. (2021). Novel epigenetic clock for fetal brain development predicts prenatal age for cellular stem cell models and derived neurons. Mol Brain *14*, 98. 10.1186/s13041-021-00810-w.
46. Peters, T.J., Buckley, M.J., Statham, A.L., Pidsley, R., Samaras, K., Lord, R.V., Clark, S.J., and Molloy, P.L. (2015). De novo identification of differentially methylated regions in the human genome. Epigenetics & Chromatin *8*. https://doi.org/10.1186/1756-8935-8-6.
47. Kolberg, L., Raudvere, U., Kuzmin, I., Adler, P., Vilo, J., and Peterson, H. (2023). g:Profiler-interoperable web service for functional enrichment analysis and gene identifier mapping (2023 update). Nucleic Acids Res *51*, W207-W212. 10.1093/nar/gkad347.
48. Shannon, P., Markiel, A., Ozier, O., Baliga, N.S., Wang, J.T., Ramage, D., Amin, N., Schwikowski, B., and Ideker, T. (2003). Cytoscape: a software environment for integrated models of biomolecular interaction networks. Genome Res *13*, 2498-2504. 10.1101/gr.1239303.
49. Davis CA, N.-T.S., Rossant J, Joyner AL (1988). Expression of the homeo box-containing gene En-2 delineates a specific region of the developing mouse brain. Genes Dev. *2*, 361-371. 10.1101/gad.2.3.361.
50. Frantz GD, W.J., Levin ME, McConnell SK (1994). Otx1 and Otx2 define layers and regions in developing cerebral cortex and cerebellum. J Neurosci *14*, 5725-5740. 10.1523/JNEUROSCI.14-10-05725.1994.

51. Englund, C., Kowalczyk, T., Daza, R.A., Dagan, A., Lau, C., Rose, M.F., and Hevner, R.F. (2006). Unipolar brush cells of the cerebellum are produced in the rhombic lip and migrate through developing white matter. J Neurosci *26*, 9184-9195. 10.1523/JNEUROSCI.1610-06.2006.
52. Badodi, S., and Marino, S. (2022). Epigenetic mechanisms in paediatric brain tumours: regulators lose control. Biochem Soc Trans *50*, 167-185. 10.1042/BST20201227.
53. Kulis, M., and Esteller, M. (2010). DNA Methylation and Cancer. In Epigenetics and Cancer, Part A, pp. 27-56. 10.1016/b978-0-12-380866-0.60002-2.
54. Gabbutt, C., Schenck, R.O., Weisenberger, D.J., Kimberley, C., Berner, A., Household, J., Lakatos, E., Robertson-Tessi, M., Martin, I., Patel, R., et al. (2022). Fluctuating methylation clocks for cell lineage tracing at high temporal resolution in human tissues. Nature Biotechnology *40*, 720-730. 10.1038/s41587-021-01109-w.
55. Vladoiu, M.C., El-Hamamy, I., Donovan, L.K., Farooq, H., Holgado, B.L., Sundaravadanam, Y., Ramaswamy, V., Hendrikse, L.D., Kumar, S., Mack, S.C., et al. (2019). Childhood cerebellar tumours mirror conserved fetal transcriptional programs. Nature *572*, 67-73. 10.1038/s41586-019-1158-7.
56. van Bree, N.F.H.N., and Wilhelm, M. (2022). The Tumor Microenvironment of Medulloblastoma: An Intricate Multicellular Network with Therapeutic Potential. Cancers *14*. 10.3390/cancers14205009.
57. Badodi, S., Pomella, N., Lim, Y.M., Brandner, S., Morrison, G., Pollard, S.M., Zhang, X., Zabet, N.R., and Marino, S. (2022). Combination of BMI1 and MAPK/ERK inhibitors is effective in medulloblastoma. Neuro Oncol. 10.1093/neuonc/noac052.
58. Silva, T.P., Sousa-Luis, R., Fernandes, T.G., Bekman, E.P., Rodrigues, C.A.V., Vaz, S.H., Moreira, L.M., Hashimura, Y., Jung, S., Lee, B., et al. (2021). Transcriptome profiling of human pluripotent stem cell-derived cerebellar organoids reveals faster commitment under dynamic conditions. Biotechnol Bioeng *118*, 2781-2803. 10.1002/bit.27797.
59. Williamson, D., Schwalbe, E.C., Hicks, D., Aldinger, K.A., Lindsey, J.C., Crosier, S., Richardson, S., Goddard, J., Hill, R.M., Castle, J., et al. (2022). Medulloblastoma group 3 and 4 tumors comprise a clinically and biologically significant expression continuum reflecting human cerebellar development. Cell Rep *40*, 111162. 10.1016/j.celrep.2022.111162.
60. Pine, A.R., Cirigliano, S.M., Nicholson, J.G., Hu, Y., Linkous, A., Miyaguchi, K., Edwards, L., Singhania, R., Schwartz, T.H., Ramakrishna, R., et al. (2020). Tumor Microenvironment Is Critical for the Maintenance of Cellular States Found in Primary Glioblastomas. Cancer Discov *10*, 964-979. 10.1158/2159-8290.CD-20-0057.
61. Yang, J., Kim, S.K., Wang, K.C., Kim, K.H., Park, S.H., and Phi, J.H. (2021). A boy with a congenital cerebellar mass. Childs Nerv Syst *37*, 983-987. 10.1007/s00381-020-04767-4.
62. Moradi, B., Hamidian, Y., Soltanghoraee, H., and Katouli, F.S. (2023). Prenatally detected congenital medulloblastoma. J Clin Ultrasound *51*, 432-435. 10.1002/jcu.23278.
63. Nicholson, J.G., Cirigliano, S., Singhania, R., Haywood, C., Shahidi Dadras, M., Yoshimura, M., Vanderbilt, D., Liechty, B., and Fine, H.A. (2024). Chronic hypoxia remodels the tumor microenvironment to support glioma stem cell growth. Acta Neuropathol Commun *12*, 46. 10.1186/s40478-024-01755-6.

64. Qu, F., Brough, S.C., Michno, W., Madubata, C.J., Hartmann, G.G., Puno, A., Drainas, A.P., Bhattacharya, D., Tomasich, E., Lee, M.C., et al. (2023). Crosstalk between small-cell lung cancer cells and astrocytes mimics brain development to promote brain metastasis. Nat Cell Biol *25*, 1506-1519. 10.1038/s41556-023-01241-6.
65. Arai, Y., Pulvers, J.N., Haffner, C., Schilling, B., Nusslein, I., Calegari, F., and Huttner, W.B. (2011). Neural stem and progenitor cells shorten S-phase on commitment to neuron production. Nat Commun *2*, 154. 10.1038/ncomms1155.
66. Srinivasan, E.S., Deshpande, K., Neman, J., Winkler, F., and Khasraw, M. (2021). The microenvironment of brain metastases from solid tumors. Neurooncol Adv *3*, v121-v132. 10.1093/noajnl/vdab121.
67. Venkatesh, H.S., Johung, T.B., Caretti, V., Noll, A., Tang, Y., Nagaraja, S., Gibson, E.M., Mount, C.W., Polepalli, J., Mitra, S.S., et al. (2015). Neuronal Activity Promotes Glioma Growth through Neuroligin-3 Secretion. Cell *161*, 803-816. 10.1016/j.cell.2015.04.012.
68. Venkatesh, H.S., Tam, L.T., Woo, P.J., Lennon, J., Nagaraja, S., Gillespie, S.M., Ni, J., Duveau, D.Y., Morris, P.J., Zhao, J.J., et al. (2017). Targeting neuronal activity-regulated neuroligin-3 dependency in high-grade glioma. Nature *549*, 533-537. 10.1038/nature24014.
69. Venkatesh, H.S., Morishita, W., Geraghty, A.C., Silverbush, D., Gillespie, S.M., Arzt, M., Tam, L.T., Espenel, C., Ponnuswami, A., Ni, L., et al. (2019). Electrical and synaptic integration of glioma into neural circuits. Nature *573*, 539-545. 10.1038/s41586-019-1563-y.
70. Taylor, L., Wade, P.K., Johnson, J.E.C., Aldighieri, M., Morlando, S., Di Leva, G., Kerr, I.D., and Coyle, B. (2023). Drug Resistance in Medulloblastoma Is Driven by YB-1, ABCB1 and a Seven-Gene Drug Signature. Cancers (Basel) *15*. 10.3390/cancers15041086.
71. Hayden Gephart, M.G., Su, Y.S., Bandara, S., Tsai, F.C., Hong, J., Conley, N., Rayburn, H., Milenkovic, L., Meyer, T., and Scott, M.P. (2013). Neuropilin-2 contributes to tumorigenicity in a mouse model of Hedgehog pathway medulloblastoma. J Neurooncol *115*, 161-168. 10.1007/s11060-013-1216-1.
72. Liu, H., Sun, Y., O'Brien, J.A., Franco-Barraza, J., Qi, X., Yuan, H., Jin, W., Zhang, J., Gu, C., Zhao, Z., et al. (2020). Necroptotic astrocytes contribute to maintaining stemness of disseminated medulloblastoma through CCL2 secretion. Neuro Oncol *22*, 625-638. 10.1093/neuonc/noz214.
73. Liang, K.H., Chang, C.C., Wu, K.S., Yu, A.L., Sung, S.Y., Lee, Y.Y., Liang, M.L., Chen, H.H., Fen, J.J., Chao, M.E., et al. (2021). Notch signaling and natural killer cell infiltration in tumor tissues underlie medulloblastoma prognosis. Sci Rep *11*, 23282. 10.1038/s41598-021-02651-y.
74. Low, S.Y.Y., Bte Syed Sulaiman, N., Tan, E.E.K., Ng, L.P., Kuick, C.H., Chang, K.T.E., Tang, P.H., Wong, R.X., Looi, W.S., Low, D.C.Y., and Seow, W.T. (2020). Cerebrospinal fluid cytokines in metastatic group 3 and 4 medulloblastoma. BMC Cancer *20*, 554. 10.1186/s12885-020-07048-0.